Annals of Physics 383 (2017) 33–78

Contents lists available at ScienceDirect

Annals of Physics

journal homepage: www.elsevier.com/locate/aop

Model dynamics for quantum computing

Frank Tabakin

Department of Physics and Astronomy, University of Pittsburgh, PA 15260, USA

HIGHLIGHTS

- General realistic density matrix evolution model shown for one qubit.
- Unitary pulses & bias yield quantum gates without harmful phase accumulations.
- Gate friction, dissipation included by random Lindblad noise pulses.
- Bath & entropy terms yield equilibrium; test algorithms, gates act on Larmor grid.
- Measurement modeled by strong, fast Lindblad pulses.

ARTICLE INFO

Article history:
Received 1 November 2016
Accepted 28 April 2017
Available online 16 May 2017

ABSTRACT

A model master equation suitable for quantum computing dynamics is presented. In an ideal quantum computer (QC), a system of qubits evolves in time unitarily and, by virtue of their entanglement, interfere quantum mechanically to solve otherwise intractable problems. In the real situation, a QC is subject to decoherence and attenuation effects due to interaction with an environment and with possible short-term random disturbances and gate deficiencies. The stability of a QC under such attacks is a key issue for the development of realistic devices. We assume that the influence of the environment can be incorporated by a master equation that includes unitary evolution with gates, supplemented by a Lindblad term. Lindblad operators of various types are explored; namely, steady, pulsed, gate friction, and measurement operators. In the master equation, we use the Lindblad term to describe short time intrusions by random Lindblad pulses. The phenomenological master equation is then extended to include a nonlinear Beretta term that describes the evolution of a closed system with increasing entropy. An external Bath environment is stipulated by a fixed temperature in two different ways. Here we explore the case of a simple one-qubit system in preparation for generalization to multi-qubit, qutrit and hybrid qubit–qutrit systems. This model master

E-mail address: tabakin@pitt.edu.

http://dx.doi.org/10.1016/j.aop.2017.04.013
0003-4916/© 2017 Elsevier Inc. All rights reserved.

equation can be used to test the stability of memory and the efficacy of quantum gates. The properties of such hybrid master equations are explored, with emphasis on the role of thermal equilibrium and entropy constraints. Several significant properties of time-dependent qubit evolution are revealed by this simple study.
© 2017 Elsevier Inc. All rights reserved.

1. Introduction

A quantum computer (QC) is a physical device that uses quantum interference to enhance the probability of getting an answer to an otherwise intractable problem [1,2]. A quantum system's ability to interfere depends on its entanglement and on maintenance of its coherent phase relations. In a real system, there are always environmental effects and also random disturbances that can cause the quantum system to lose its ability to display quantum interference. That process is called decoherence, as is discussed in an extensive literature [3] on how a quantum system becomes classical, often rapidly, due to its interaction with an external environment. That process might also be viewed as a measuring device [4,5]. A major concern in the development of a realistic quantum computer is to understand, control, and/or correct for detrimental environmental effects.

A general theory of how such "open systems" evolve in time is provided by the operator sum representation (OSR), which replaces the unitary evolution of a closed system by a more general form that accounts for the fact that the system under study (the quantum computer) is affected by an environment. That general form involves Kraus [6] operators and is often described as a mapping.

To gain insight, models for the environment and its interaction with the QC have been discussed [7]. These studies use the Dyson series for the time evolution and reduce the dynamics to the QC subsystem using a variety of approximations. One approximation, truncating the Dyson series (a Born approximation) is used since an exact solution is generally not available. An oft-used approximation is that in the system–environment interaction the environment restores itself rapidly to its initial condition, and therefore only the present situation of the environment is relevant. That is, one invokes a Markov approximation, which has the environment affecting the system, but the system's effect on the environment vanishes rapidly. It is assumed that the system and environment are initially uncorrelated and are described as a product state.

The Markov approximation is not always applicable; that depends on the dynamics of the environment and its interaction with the system. It is physically possible that the system affects an environment that is able to partially preserve that influence and feed part of it back to the system. Indeed, there are important papers that indicate that the Markov approximation is in doubt [8]. Nevertheless, our initial approach is to adopt the Markov approximation, with plans to test its applicability.

A vast literature exists on deducing a general master equation for the time evolution of a subsystem's density matrix. One method is to examine the above Dyson series methods, as described in [7]. Another approach is to replace unitary evolution,[1] by a Kraus subsystem form of evolution.[2] Then a "generalized infinitesimal" expansion of the Kraus operators is used to deduce a differential equation for the density matrix, yielding a linear in density matrix master equation. The "generalized infinitesimal" is related to Ito calculus, which involves how to define variations for stochastic, or rapidly fluctuating functions. Several papers [9,10] discuss this procedure and ways to deduce a master equation for the subsystem's density matrix, which prove to be of the form deduced earlier by Gorini, Kossakowski, Sudarshan and Lindblad [11–14], who used other general considerations. The Lindblad form can be deduced in general from requiring preservation of density matrix Hermiticity, unit trace, and positive-definite properties, without the restriction to time independent Lindblad operators or to particular initial states. The Lindblad form can be used to describe all environmental

[1] $\rho(t) = U(t)\rho(0)U^{\dagger}(t)$.

[2] $\rho(t) = \sum_{\alpha} K_{\alpha}(t)\,\rho(0)\,K_{\alpha}^{\dagger}(t)$ with $\sum_{\alpha} K_{\alpha}(t)K_{\alpha}^{\dagger} = 1$ and $\rho^{\dagger}(t) = \rho;\ \mathrm{Tr}\rho(t) = 1$.

effects. However, we introduce special terms to isolate and to gain insight into specific effects, such as the Bath–system dynamics. Lindblad's equation for the time evolution of a subsystem's density matrix has many appealing features, as discussed later.

Profound papers by Beretta [15–17] provide a general master equation based on novel concepts of non-equilibrium statistical mechanics as applied to quantum systems. The Beretta master equation for describing an open system has not been used much for QC perhaps because it is nonlinear and it alters entropy addition rules. An excellent rendition of the basic nature of the Beretta (and other nonlinear master equations) is provided in papers by Korsch et al. [18,19].

The Beretta description includes definitions of entropy, work, and heat for non-equilibrium systems. The resultant master equation has many important features, as illustrated in our study. Indeed, we incorporate the Beretta master equation for QC and extend it using a phenomenological viewpoint.

In Section 2, we discuss the basic idea of a density matrix from two traditional points of view. One view is to form a classical ensemble average over an ensemble of quantum systems. The second viewpoint is that a single quantum system is prepared in a state averaged over its production possibilities. After discussing general properties of the density matrix, we stress that the dynamics of the density matrix can be best visualized in terms of the time development of its spin polarization and spin correlation observables.

In Section 3, we describe how the density matrix evolves by unitary evolution driven by a time-dependent Hamiltonian that includes level splitting and ideal gate pulses. During a gate pulse, a bias pulse is used to impose temporary degeneracy to halt precession and avoid awkward phase accumulation. Then a model master equation is introduced in Section 4 along with an analysis of its several terms. These terms are: (1) Lindblad form used to include random noise and gate friction effects, (2) a Beretta term to describe a closed-system with increasing entropy, and (3) a Bath term for contact with an environment of specific temperature. We make a heuristic assumption that the Lindblad and Beretta forms are both useful, and we adopt a phenomenological or hybrid viewpoint. That viewpoint, which is not derived but postulated, is to use Lindblad terms to describe random, short-time intrusions on the QC, which could be caused by for example a passing particle. And we use the nonlinear Beretta term to describe the overall trend for a closed system to steadily increase in entropy. A Beretta description of Bath–system (open) dynamics is also included. The system is simultaneously driven towards equilibrium with an environment or bath of a specified temperature. On top of these major effects, we describe the time-evolution of quantum gates by Hamiltonian pulses. If the Lindblad and Bath terms are both set to zero, which is equivalent to removing the environment, and the closed-system Beretta term is omitted, then the master equation reduces necessarily to ordinary unitary evolution.

In Section 4.3, we introduce the Lindblad master equation and discuss several aspects of its general features, and limitations. We then proceed to a similar analysis of the Beretta and Bath terms 4.4. Finally, in Section 5 properties of the full master equation are examined and conclusions and future plans are stated in Section 6.

The above assumptions provide a practical dynamic framework for examining not only the influence of an environment on the efficacy of a QC, but also the loss of reliability in the action of gates or the general loss of coherence. The master equation we design incorporates the main features of a density matrix; namely, Hermiticity, unit trace and positive definite character, while also including the evolution of a closed system and the effects of gates, noise and of an external bath.

2. Density operator

The density operator, also called a density matrix, is an operator in Hilbert space that represents an ensemble of quantum systems. As introduced by von Neumann and Landau [20–22], the density operator, ρ, can be understood as a classical ensemble average over a collection of subsystems (the ensemble) which occur in a general state $|\alpha\rangle$, with a probability $\mathscr{P}_\alpha$. By a general state, we mean a state of the subsystem that is a general superposition of a complete orthonormal basis (such as eigenstates

of a Hamiltonian). For the simple case of an ensemble of spin 1/2 particles, such a state called a qubit is specified by the spinor

$$|\alpha\rangle = |\hat{n}_\alpha\rangle = \cos(\theta_\alpha/2)e^{-i\phi_\alpha/2}|0\rangle + \sin(\theta_\alpha/2)e^{+i\phi_\alpha/2}|1\rangle = \begin{pmatrix}\cos(\theta_\alpha/2)e^{-i\phi_\alpha/2}\\ \sin(\theta_\alpha/2)e^{+i\phi_\alpha/2}\end{pmatrix}, \tag{1}$$

where the computational bases $|0\rangle$ and $|1\rangle$ denote spin-up and spin-down states, respectively, and α labels the Euler angles θ_α, ϕ_α, that specify a general direction $\hat{n}_\alpha$ in which the qubit is pointing. Indeed, the above state is an eigenstate of the operator $\vec{\sigma}\cdot\hat{n}_\alpha$, where the components of $\vec{\sigma}$ are the Pauli operators (see below). This description is readily generalized to multiparticle qubit states and also to systems that are doublets without being associated with the idea of physical spin.

The above general state is normalized but not necessarily orthogonal, $\langle\alpha'|\alpha\rangle \neq \delta_{\alpha',\alpha}$. The quantum rule for the expectation value of a general operator Ω, is $\langle\alpha|\Omega|\alpha\rangle$ and for an ensemble of separate quantum subsystems one can form the classical ensemble average $\langle\Omega\rangle$ for the Hermitian observable Ω by taking

$$\langle\Omega\rangle = \frac{\sum_\alpha \langle\alpha|\Omega|\alpha\rangle \mathscr{P}_\alpha}{\sum_\alpha \mathscr{P}_\alpha}. \tag{2}$$

The ensemble average is then a simple classical average where $\mathscr{P}_\alpha$ is the probability that a particular state α appears in the ensemble. Summing over all possible states of course yields $\sum_\alpha \mathscr{P}_\alpha = 1$. The above expression is a combination of a classical ensemble average with the quantum mechanical expectation value. It contains the idea that each member of the ensemble interferes only with itself quantum mechanically and that the ensemble involves a simple classical average over the probability distribution of the ensemble.

We now define the **density operator** by

$$\rho \equiv \sum_\alpha |\alpha\rangle\langle\alpha|\mathscr{P}_\alpha. \tag{3}$$

Using closure,[3] the ensemble average can now be expressed as a ratio of traces

$$\langle\Omega\rangle = \frac{\mathrm{Tr}(\rho\,\Omega)}{\mathrm{Tr}(\rho)} \equiv \mathrm{Tr}(\rho\,\Omega), \tag{4}$$

which entails the properties

$$\begin{aligned}\mathrm{Tr}(\rho) &= \sum_m \langle m|\rho|m\rangle = \sum_\alpha \mathscr{P}_\alpha \sum_m \langle\alpha|m\rangle\langle m|\alpha\rangle\\ &= \sum_\alpha \mathscr{P}_\alpha \langle\alpha|\alpha\rangle = \sum_\alpha \mathscr{P}_\alpha = 1,\end{aligned} \tag{5}$$

where $|m\rangle$ denotes a complete orthonormal basis (such as the computational basis), and

$$\begin{aligned}\mathrm{Tr}(\rho\,\Omega) &= \sum_{mm'} \langle m|\rho|m'\rangle\langle m'|\Omega|m\rangle\\ &= \sum_\alpha \sum_{mm'} \mathscr{P}_\alpha \langle\alpha|m'\rangle\langle m'|\Omega|m\rangle\langle m|\alpha\rangle\\ &= \sum_\alpha \mathscr{P}_\alpha \langle\alpha|\Omega|\alpha\rangle,\end{aligned} \tag{6}$$

which returns the original ensemble average expression.

[3] The closure property, which is a statement that $|n\rangle$ is a complete orthonormal basis, is $\sum_n |n\rangle\langle n| = 1$.

2.1. Properties of the density matrix

The definition $\rho = \sum_\alpha |\alpha\rangle\langle\alpha|\mathscr{P}_\alpha$ is a general one, if we interpret α as the label for the possible characteristics of a state. Several important general properties of a density operator follow from this definition. The density operator is:

- Hermitian $\rho^\dagger \equiv \rho$, hence its eigenvalues are real;
- has unit trace, $\mathrm{Tr}(\rho) \equiv 1$, hence the sum of its eigenvalues equals 1;
- is positive definite, which means that all of its eigenvalues are greater or equal to zero. This, together with the fact that the density matrix has unit trace, ensures that each eigenvalue is between zero and one, and yet sum to 1;
- for a pure state, every member of the ensemble has the same quantum state and only one α_0 appears and the density operator becomes $\rho = |\alpha_0\rangle\langle\alpha_0|$. The state $|\alpha_0\rangle$ is normalized to one and hence for a pure state $\rho^2 = \rho$. Thus for a pure state one of the density matrix eigenvalues is 1, with all others zero;
- for a general ensemble $\rho^2 \leq \rho$ which has a mixture of possibilities as reflected in the probability distribution $\mathscr{P}_\alpha$ with the equal sign holding for pure states.

2.1.1. Composite systems and partial trace

For a composite system, such as an ensemble of quantum systems each of which is prepared with a probability distribution, the definition of a density matrix can be generalized to a product Hilbert space form involving systems of types A and B

$$\rho_{AB} \equiv \sum_{\alpha,\beta} \mathscr{P}_{\alpha,\beta}|\alpha\beta\rangle\langle\alpha\beta|, \tag{7}$$

where $\mathscr{P}_{\alpha,\beta}$ is the joint probability for finding the two systems with the attributes labeled by α and β. For example, α could designate the possible directions $\hat{n}_\alpha$ of one spin-1/2 system, while β labels the possible spin directions of another spin 1/2 system, $\hat{n}_\beta$. One can always ask about the state of just system A or B by summing over or tracing out the other system. For example, the density matrix of system A is picked out of the general definition above by the following partial trace steps

$$\begin{aligned}
\rho_A &= \mathrm{Tr}_B(\rho_{AB}) \\
&= \sum_{\alpha,\beta} \mathscr{P}_{\alpha,\beta}|\alpha\rangle\langle\alpha|\mathrm{Tr}_B\Big[|\beta\rangle\langle\beta|\Big] \\
&= \sum_\alpha \Big(\sum_\beta \mathscr{P}_{\alpha,\beta}\Big)|\alpha\rangle\langle\alpha| \\
&= \sum_\alpha \mathscr{P}_\alpha|\alpha\rangle\langle\alpha|.
\end{aligned} \tag{8}$$

Here we use the product space $|\alpha\beta\rangle \mapsto |\alpha\rangle|\beta\rangle$ and we define the probability for finding system A in situation α by

$$\mathscr{P}_\alpha = \sum_\beta \mathscr{P}_{\alpha,\beta}. \tag{9}$$

This is a standard way to get an individual probability from a joint probability.

It is easy to show that all of the other properties of a density matrix still hold true for a composite system case. It has unit trace, it is Hermitian with real eigenvalues and is positive definite.

2.2. Comments about the density matrix

2.2.1. Alternate views of the density matrix

In the prior discussion, the view was taken that the density matrix implements a classical average over an ensemble of many quantum systems, each member of which interferes quantum mechanically

only with itself. An alternate equally valid viewpoint is that a single quantum system is prepared, but the preparation of this single system is not pinned down. Instead all we know is that it is prepared in any one of the states labeled again by a generic state label α with a probability $\mathscr{P}_\alpha$. Despite the change in interpretation, or rather an application to a different situation, all of the properties and expressions presented for the ensemble average hold true; only the meaning of the probability is altered.

An important point concerning the density matrix is that the ensemble average (or the average expected result for a single system prepared as described in the previous paragraph) can be used to obtain these averages for all observables Ω. Hence in a sense the density matrix describes a system and the system's accessible observable quantities. It represents then an honest statement of what we can really know about a system. On the other hand, in Quantum Mechanics it is the wave function that tells all about a system. Clearly, since a density matrix is constructed as a weighted average over bilinear products of wave functions, the density matrix has less detailed information about a system than is contained in its wave function. Explicit examples of these general remarks will be given later.

To some authors the fact that the density matrix has less content than the system's wave function, causes them to avoid use of the density matrix. Others find the density matrix description of accessible information as appealing. Indeed, S. Weinberg in recent papers [23,24] has advocated an interpretation of quantum mechanics based on using the density matrix rather than the state vector as a description of reality. The attribution of such deep physical meaning to the density operator was advocated earlier by Hatsopoulos and Gyftopoulos [25], who inspired by a deep analysis by Park [26] on the nature of quantum states, adopted it as the key physical ansatz of their early theory of quantum thermodynamics, which in turn prompted Beretta to design the nonlinear master equation that we adopt below as part of our model master equation.

We now turn to discussing the basic features of the density matrix in preparation for describing its dynamic evolution by means of a model master equation.

2.2.2. Classical correlations and entanglement

The density matrix for composite systems can take many forms depending on how the systems are prepared. For example, if distinct systems A & B are independently produced and observed independently, then the density matrix is of product form $\rho_{AB} \mapsto \rho_A \otimes \rho_B$, and the observables are also of product form $\Omega_{AB} \mapsto \Omega_A \otimes \Omega_B$. For such an uncorrelated situation, the ensemble average factors

$$\langle \Omega_{AB} \rangle = \frac{\mathrm{Tr}(\rho_{AB}\Omega_{AB})}{\mathrm{Tr}(\rho_{AB})} = \frac{\mathrm{Tr}(\rho_A\Omega_A)}{\mathrm{Tr}(\rho_A)} \frac{\mathrm{Tr}(\rho_B\Omega_B)}{\mathrm{Tr}(\rho_B)} = \langle \Omega_A \rangle \langle \Omega_B \rangle, \tag{10}$$

as is expected for two separate uncorrelated experiments. This can also be expressed as having the joint probability factor $\mathscr{P}_{\alpha,\beta} \mapsto \mathscr{P}_\alpha \mathscr{P}_\beta$ the usual probability rule for uncorrelated systems.

Another possibility for the two systems is that they are prepared in a coordinated manner, with each possible situation assigned a probability based on the correlated preparation technique. For example, consider two colliding beams, A & B, made up of particles with the same spin. Assume the particles are produced in matched pairs with common spin direction $\hat{n}$. Also assume that the preparation of that pair in that shared direction is produced by design with a classical probability distribution $\mathscr{P}_{\hat{n}}$. Each pair has a density matrix $\rho_{\hat{n}} \otimes \rho_{\hat{n}}$ since they are produced separately, but their spin directions are correlated classically. The density matrix for this situation is then

$$\rho_{AB} = \sum_{\hat{n}} \mathscr{P}_{\hat{n}}\, \rho_{\hat{n}} \otimes \rho_{\hat{n}}. \tag{11}$$

This is a "mixed state" which represents classically correlated preparation and hence any density matrix that can take on the above form can be reproduced by a setup using classically correlated preparations and does *not* represent the essence of Quantum Mechanics, e.g. an entangled state.

An entangled quantum state is described by a density matrix (or by its corresponding state vectors) that is not and cannot be transformed into the two classical forms above; namely, cast into a product or a mixed form. For example, the two-qubit Bell state $\frac{1}{\sqrt{2}}(|01\rangle + |10\rangle)$ has a density matrix

$$\rho = \frac{1}{2}(|01\rangle\langle 01| + |01\rangle\langle 10| + |10\rangle\langle 01| + |10\rangle\langle 10|) \tag{12}$$

that is not of simple product or mixed form. It is the prime example of an entangled state.

The basic idea of decoherence can be described by considering the above Bell state case with time dependent coefficients

$$\rho = \frac{1}{2}(a_1(t)|01\rangle\langle 01| + a_2(t)|01\rangle\langle 10| + a_2^*(t)|10\rangle\langle 01| + (1 - a_1(t))|10\rangle\langle 10|). \tag{13}$$

If the off-diagonal terms $a_2(t)$ vanish, by attenuation and/or via time averaging, then the above density matrix does reduce to the mixed or classical form,

$$\rho = \frac{1}{2}(a_1(t)|01\rangle\langle 01| + (1 - a_1(t))|10\rangle\langle 10|), \tag{14}$$

which is an illustration of how decoherence leads to a classical state.

2.3. Observables and the density matrix

Visualization of the density matrix and understanding its significance is greatly enhanced by defining associated real spin observables. In the simplest one-qubit case, the density matrix is a 2×2 Hermitian positive definite matrix of unit trace. Thus it is fully stipulated by three real parameters, which are identified as the polarization vector $\vec{P}(t)$, also called the Bloch vector. One can deduce that only three parameters are needed for the one-qubit case from the following steps: (1) a general 2×2 matrix with complex entries involves $2(2 \times 2) = 8$ real numbers; (2) the Hermitian condition reduces the diagonal terms to 2 and the off-diagonal terms to 2, a net of 4 remaining real numbers; (3) the unit trace reduces the count by 1, so we have $4 - 3 = 3$ parameters. These steps generalize to multi-qubit and to qutrit cases.

Operators or gates acting on a single qubit state are represented by 2×2 matrices. The dimension of the single qubit state vectors ($|0\rangle$ and $|1\rangle$) is $N = 2^{n_q} = 2$, with $n_q = 1$. The Pauli matrices provide an operator basis of all such matrices. The Pauli-spin matrices are:

$$\sigma_0 = \begin{pmatrix} 1 & 0 \\ 0 & 1 \end{pmatrix}, \sigma_1 = \begin{pmatrix} 0 & 1 \\ 1 & 0 \end{pmatrix}, \sigma_2 = \begin{pmatrix} 0 & -i \\ i & 0 \end{pmatrix}, \sigma_3 = \begin{pmatrix} 1 & 0 \\ 0 & -1 \end{pmatrix}. \tag{15}$$

These are all Hermitian traceless matrices $\sigma_i = \sigma_i^\dagger$. We use the labels $(1, 2, 3)$ to denote the directions (x, y, z). The fourth Pauli matrix σ_0 is simply the unit matrix. Any 2×2 matrix can be constructed from these four Pauli matrices, which therefore are an operator basis, also called the computational basis operators. That construction applies to the density matrix $\rho(t)$ at any time t and to the Hamiltonian $H(t)$, and Lindblad operators $L(t)$.

2.3.1. Polarization

The general form of a one-qubit density matrix, using the 4 Hermitian Pauli matrices as an operator basis is:

$$\begin{aligned} \rho(t) &= \frac{1}{2}\Big[\sigma_0 + P_1(t)\,\sigma_1 + P_2(t)\,\sigma_2 + P_3(t)\,\sigma_3\Big] \\ &= \frac{1}{2}\Big[\sigma_0 + \vec{P}(t)\cdot\vec{\sigma}\Big] \\ &= \frac{1}{2}\begin{pmatrix} 1 + P_3(t) & P_1(t) - iP_2(t) \\ P_1(t) + iP_2(t) & 1 - P_3(t) \end{pmatrix}, \end{aligned} \tag{16}$$

where the spin operators are $\vec{\sigma} = \{\vec{\sigma}_1, \vec{\sigma}_2, \vec{\sigma}_3\}$, and the real polarization vector is $\vec{P}(t) = \{P_1(t), P_2(t), P_3(t)\}$. The polarization, $\vec{P}(t)$ is a real vector, which follows from the Hermiticity of the density matrix $\rho^\dagger(t) \equiv \rho(t)$ and from the ensemble average relation

$$\vec{P}(t) = \mathrm{Tr}(\vec{\sigma}\cdot\rho(t)) \equiv \langle\vec{\sigma}\rangle.$$

Thus specifying the polarization vector (also called the Bloch vector) determines the density matrix and it is convenient to view the polarization as a function of time to gain insight into qubit dynamics.

The above expression clearly satisfies the density matrix conditions that $\mathrm{Tr}(\rho(t)) = 1$, $\rho^\dagger(t) = \rho(t)$. The positive definite condition follows from determining that the two eigenvalues are $\lambda_1(t) = \frac{1+\mathbf{P}(t)}{2}$, $\lambda_2 = \frac{1-\mathbf{P}(t)}{2}$, where $\mathbf{P}(t) = \sqrt{P_1(t)^2 + P_2(t)^2 + P_3(t)^2} \leq 1$. The unit trace condition becomes simply that the eigenvalues of ρ sum to one

$$\begin{aligned} \mathrm{Tr}(\rho(t)) = 1 &= \mathrm{Tr}(U_\rho(t) \cdot \rho_D(t) \cdot U_\rho^\dagger(t)) \\ &= \mathrm{Tr}((U_\rho^\dagger(t) \cdot U_\rho(t)) \cdot \rho_D(t)) \\ &= \mathrm{Tr}(\rho_D(t)) \\ &= \lambda_1(t) + \lambda_2(t), \end{aligned} \tag{17}$$

where $U_\rho(t)$ is the unitary matrix that diagonalizes the density matrix at time t. The diagonal density matrix $\rho_D(t)$ has real eigenvalues along the diagonal. The positive definite condition now asserts that each of these eigenvalues is greater or equal to zero and less than or equal to one: $0 \leq \lambda_i(t) \leq 1$, while summing to 1. For the one qubit case the above conditions mean that $\lambda_1(t) + \lambda_2(t) = 1$, and since $0 \leq \lambda_i(t) \leq 1$, the polarization vector must have a length between zero and one.

Note that the density matrix, polarization vector and its eigenvalues in general depend on time. Indeed, the dynamics of a one-qubit system is best visualized by how the polarization or eigenvalues change in time.

The polarization operator is simply $\Omega = \vec{\sigma}$ and we have the following relations for the value and time derivative of the polarization vector:

$$\begin{aligned} \vec{P}(t) &= \mathrm{Tr}(\vec{\sigma} \cdot \rho(t)) = \langle \vec{\sigma} \rangle \\ \frac{d\vec{P}(t)}{dt} &= \mathrm{Tr}\Big(\vec{\sigma} \cdot \frac{d\rho(t)}{dt}\Big). \end{aligned} \tag{18}$$

Much of what is presented here applies to multi-qubit and qutrit cases. The main difference for more qubits/qutrits is an increase in the number of polarization and spin correlation observables.

Several other quantities are used to monitor the changing state of a quantum system. Later energy, power, heat transfer and temperature concepts will be discussed. Next purity, fidelity, and entropy attributes will be examined.

2.3.2. Purity

The purity $\mathcal{P}(t)$ is defined as $\mathcal{P}(t) = \langle \rho(t) \rangle = \mathrm{Tr}(\rho(t)\,\rho(t))$. It is called purity since for a pure state density matrix $\rho = |\psi\rangle\langle\psi|$, $\rho^2 = \rho$ and $\mathrm{Tr}(\rho^2) = \mathrm{Tr}(\rho) = 1$, but in general $\mathrm{Tr}(\rho^2) \leq 1$. For a pure state, we see that $\rho^2 = \rho$, implies that each eigenvalue satisfies $\lambda_i(\lambda_i - 1) = 0$, so $\lambda_i = 0$ or 1. Since the eigenvalues sum to 1, a pure state has one eigenvalue equal to one, all others are zero. A mixed or impure state has $\sum_{i=1,2^{n_q}} \lambda_i^2 < 1$, which indicates that the nonzero eigenvalues are less than 1.

For a one-qubit system, the purity is simply related to the polarization vector

$$\begin{aligned} \mathcal{P}(t) &= \mathrm{Tr}(\rho^2(t)) = \frac{1 + \mathbf{P}^2(t)}{2}, \\ \frac{d\mathcal{P}(t)}{dt} &= 2\,\mathrm{Tr}\Big(\rho(t)\,\frac{d\rho(t)}{dt}\Big) = \vec{P}(t) \cdot \frac{d}{dt}\vec{P}(t), \end{aligned} \tag{19}$$

where $\mathbf{P}(t)$ is the length of the polarization vector $\vec{P}(t)$. Thus a pure state has a polarization vector that is on the unit Bloch sphere, whereas an impure state's polarization vector is inside the Bloch sphere. The purity ranges from a minimum of 0.5 to a maximum of 1. Later we will see how dissipation and entropy changes can bring the polarization inside the Bloch sphere and hence generate impurity.

2.3.3. Fidelity

Fidelity measures the closeness of two states. In its simplest form, this quantity can be defined as $\mathscr{F}^2 = \mathrm{Tr}[\rho_A\,\rho_B]$. For the special case that $\rho_A = |\psi_A\rangle\langle\psi_A|$ & $\rho_B = |\psi_B\rangle\langle\psi_B|$, this yields $\mathscr{F} \equiv |\langle\psi_A|\psi_B\rangle|$, which is clearly the magnitude of the overlap probability amplitude.

To align the quantum definition of fidelity with classical probability theory, a more general definition is invoked; namely,

$$\mathscr{F}(\rho_A, \rho_B) \equiv \mathrm{Tr}\Big[\sqrt{\sqrt{\rho_A}\ \rho_B\ \sqrt{\rho_A}}\Big]. \tag{20}$$

When ρ_A and ρ_B commute, they can both be diagonalized by the same unitary matrix, but with different eigenvalues. In that limit, we have $\rho_A = \sum_i \lambda_i^A |i\rangle\langle i|$ & $\rho_B = \sum_j \lambda_j^B |j\rangle\langle j|$ and

$$\mathscr{F}(\rho_A, \rho_B) \equiv \mathrm{Tr}\Big[\sqrt{\rho_A\ \rho_B}\Big] \equiv \sum_{i,j} \sqrt{\lambda_i^A \lambda_j^B}, \tag{21}$$

which is the classical limit result.

We will use fidelity to monitor the efficacy or stability of any QC process, where $\rho_A(t)$ is taken as the exact result and $\rho_B(t)$ is the result including decoherence, gate friction, and dissipation effects.

2.3.4. Entropy

The Von Neumann [20] entropy at time t is defined by

$$S(t) = -\mathrm{Tr}(\rho(t)\ \log_2\ \rho(t)). \tag{22}$$

The Hermitian density matrix can be diagonalized by a unitary matrix $U_\rho(t)$ at time t,

$$\rho(t) = U_\rho(t)\ \rho^D(t)\ U_\rho^\dagger(t),$$

where $\rho_D(t)$ is diagonal matrix $\rho^D(t)_{i,j} = \delta_{i,j}\lambda_i$ of the eigenvalues. Then

$$S(t) = -(\lambda_1\ \log_2\ \lambda_1 + \lambda_2\ \log_2\ \lambda_2). \tag{23}$$

With a base 2 logarithm, the maximum entropy for one qubit is $S_{max} \equiv 1$ which occurs when the two eigenvalues are all equal to $1/2$. That is the most chaotic, or least information situation. The minimum entropy of zero obtains when one eigenvalue is one, all others being zero; that is the most organized, maximum information situation. For one qubit, zero entropy places the polarization vector on the Bloch sphere, where the length of the polarization vector is one. If the polarization vector moves inside the Bloch sphere, entropy increases. For n_q qubits entropy ranges between zero and n_q.

For later use, consider the time derivative of the entropy

$$\begin{aligned}\frac{dS}{dt} &= -\sum_{i=1,2}\Big(\frac{d\lambda_i}{dt}\log_2(\lambda_i) + \frac{d\lambda_i}{dt}\Big)\\ &= -\mathrm{Tr}\Big(\frac{d\rho}{dt}\log_2(\rho(t))\Big).\end{aligned} \tag{24}$$

Since $\mathrm{Tr}(\rho) = \sum_{i=1,2}\lambda_i \equiv 1$, the second RHS term above vanishes. Note that the above result is derived assuming that for all eigenvalues $\lambda_i/\lambda_i \to 1$, which is ambiguous for zero eigenvalues. This is no doubt related to divergences that could arise when say $\lambda_1 = 0$, and $\frac{d\lambda_1}{dt}$ is nonzero. We will confront this issue later.

Note that the eigenvalues, purity, fidelity and entropy all depend on the length of the polarization vector $\mathbf{P}(t)$.

3. First steps towards a master equation model—unitary evolution, gates and pulses

The master equation for the time evolution of the system's density matrix is now presented. We are interested in developing a simple model that incorporates the main features of the qubit dynamics for a quantum computer. These main features include seeing how the dynamics evolve under the action of gates and the role of both closed system dynamics and of open system decoherence, dissipation and the system's approach to equilibrium. From the density matrix we can determine a variety of observables, such as the polarization vector, the power and heat rates, the purity, fidelity, and entropy all as a function of time.

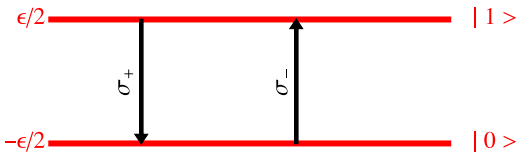

Fig. 1. Color versions of all the figures are in the web version of this article. The qubit levels with splitting $\epsilon = \hbar\,\omega_L$. With our conventions the operator $\sigma_- \equiv \frac{\sigma_x - i\sigma_y}{\sqrt{2}}$ raises the qubit to the polarization-down state $|1\rangle$, while $\sigma_+ \equiv \frac{\sigma_x + i\sigma_y}{\sqrt{2}}$ lowers the qubit to the polarization-up ground state $|0\rangle$.

3.1. Unitary evolution

We start with the observation that the density matrix for a closed system is driven by a Hamiltonian $H(t)$, that can be explicitly time dependent, as $\rho(t) = U(t)\rho(0)U^\dagger(t)$, where the unitary operator is $U(t) = e^{-\frac{i}{\hbar}H(t)\,t}$. For infinitesimal time increments this yields the unitary evolution or commutator term:

$$\frac{d\rho}{dt} = -\frac{i}{\hbar}\Big[H(t),\,\rho(t)\Big]. \tag{25}$$

This term specifies the reversible motion of a closed system. To include dissipation, an additional operator $\mathcal{L}$ will be added $\dot\rho = -\frac{i}{\hbar}\Big[H(t),\,\rho(t)\Big] + \mathcal{L}$ which describes an irreversible open system.

3.2. Hamiltonian

Our Hamiltonian $H(t) = H_0 + V(t)$ is an Hermitian operator in spin space; for one qubit it is a 2×2 matrix. It consists of a time independent H_0, plus a time dependent part $V(t)$. For $n_q = 1$, a typical Hamiltonian is

$$H_0 \equiv -\frac{1}{2}\,\hbar\,\omega_L\,\vec\sigma\cdot\hat z = -\frac{1}{2}\,\hbar\,\omega_L\,\sigma_z, \tag{26}$$

which describes a 2 level system with eigenvalues $-\frac{1}{2}\,\hbar\omega_L$ for state $|0\rangle$, and $+\frac{1}{2}\,\hbar\omega_L$ for state $|1\rangle$, see Fig. 1.

The polarization vector for this case precesses about the $\hat z$ direction with the Larmor angular frequency ω_L. This follows from the unitary evolution term

$$\begin{aligned}\frac{d\vec P(t)}{dt} &= \mathrm{Tr}\Big(\vec\sigma\;\frac{d\rho(t)}{dt}\Big)\\ &= -i\frac{\omega_L}{2}\,\mathrm{Tr}\Big[\vec\sigma\cdot[\vec\sigma\cdot\hat z,\,\rho(t)]\Big]\\ &= -\vec\omega_L\times\vec P(t),\end{aligned} \tag{27}$$

where $\vec\omega_L = \omega_L\,\hat z$, which is a Larmor precession of the polarization vector about the direction $\hat z$. The polarization vector then has a fixed value of P_z and the x and y components vary as

$$\begin{aligned}P_x(t) &= P_x(0)\cos(\omega_L t) + P_y(0)\sin(\omega_L t)\\ P_y(t) &= P_y(0)\cos(\omega_L t) - P_x(0)\sin(\omega_L t).\end{aligned} \tag{28}$$

The above is equivalent to $\dot P_i = \sum_{j=1,3} M_{i,j}P_j$, with

$$M = \begin{pmatrix} 0 & \omega_L & 0\\ -\omega_L & 0 & 0\\ 0 & 0 & 0\end{pmatrix}. \tag{29}$$

This form will be extended to dissipative cases later.

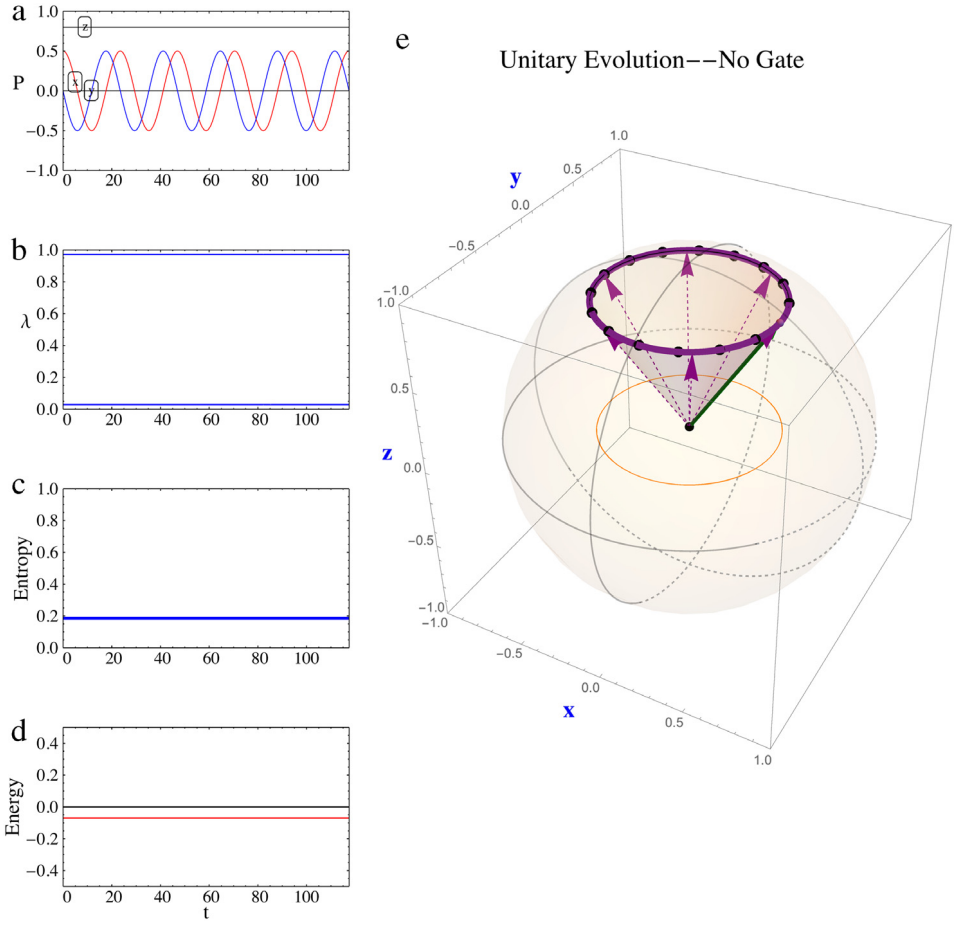

Fig. 2. Polarization vector precession (no gates and no dissipation): (a) fixed P_z and oscillating P_x, P_y components versus time, (b) the two (fixed) eigenvalues λ of $\rho(t)$, (c) the fixed entropy, and (d) the fixed energy (power and heat rate are zero). The Bloch sphere (e) with solid vector indicating the initial location of the polarization (which originates from the center of the Bloch sphere) while the subsequent motion follows the thick path as also shown by the dashed polarization vectors at subsequent times. The dots indicate equal time interval locations of the polarization vector. The precession is also projected to the x–y plane. The initial density matrix and level parameters are in Table 1.

Thus the level splitting $\hbar\omega_L$ produces a precessing polarization with a fixed z-axis value and circular motion in the x–y plane (see Fig. 2). The basic Hamiltonian H_0 is selected to be time independent. The initial density matrix and level splitting parameters used in our examples[4] are listed in Table 1. Energy is in μeV, frequency in GHz and time is in nanoseconds (ns).

Next we add a time dependence in the form of Hamiltonian pulses that produce quantum gates.

3.2.1. *One-qubit ideal gates*

For our QC application, the Hamiltonian $H(t) = H_0 + V(t)$ is used to incorporate two effects. The first is the level splitting, Eq. (26). Here ω_L denotes the Larmor angular frequency associated with the level splitting $\hbar\omega_L$, which sets the Larmor time scale $T_L = 2\pi/\omega_L$ for the system. The $V(t)$ term is used

[4] All of the numerical examples in this paper were generated by Mathematica codes based on the QDENSITY/QCWAVE packages [27].

Table 1
Initial density matrix & level parameters.

Name	Value
P_1	0.5
P_2	0.0
P_3	0.8
P	0.943
Initial Purity	0.945
Initial Entropy	0.186
Initial Temperature	0.93 mK
Larmor frequency ω_L	0.2675 GHz
Larmor Period T_L	23.5 ns
Level split $\hbar\omega_L$	0.1761 μeV

to include quantum gates Ω, which are 2×2 Hermitian matrices. For example, a single qubit NOT gate is $\Omega = \sigma_1$. The NOT acts as: $\sigma_x|0\rangle = |1\rangle$ & $\sigma_x|1\rangle = |0\rangle$. This basic gate is simply a spinor rotation about the $\hat{x}$ axis by π radians. Clearly, two NOTs return to the original state. $NOT.NOT = \sigma_1^2 = \mathcal{I}_2$.

A gate operator Ω is introduced as a Hamiltonian generator $V_G(t)$

$$V_G(t) \equiv \hbar\, \theta_G(t)\, \Omega, \tag{30}$$

where $\theta_G(t)$ is a gate pulse that is centered at time t_0 with a width τ. The pulse $\theta_G(t)$ has inverse time units. Thus the pulse essentially starts at $t_1 = t_0 - \tau/2$ and ends at $t_2 = t_0 + \tau/2$; we typically take this pulse to be of Gaussian form, $\theta_G \to \theta_g$

$$\theta_g(t) = \frac{\sqrt{\pi}}{2\tau}\, e^{-(\frac{t-t_0}{\tau})^2}. \tag{31}$$

We call $V_G(t)$ the gate generator[5] since it generates the effect of a specific gate. The pulse function $\theta_G(t)$ is designed to generate a suitable rotation over an interval t_1 to t_2. Since we want to have a smooth pulse, we take these pulses to be of either Gaussian $\theta_g(t)$ or soft square $\theta_s(t)$ shape. The soft square shape is defined by

$$\theta_s(t) = N_f\, \frac{1}{2}\left[\mathrm{Erf}\Big(\frac{t-t_1}{\tau}\Big) - \mathrm{Erf}\Big(\frac{t-t_2}{\tau}\Big)\right],$$

where N_f is fixed by the $\int_{-\infty}^{\infty} \theta_G(t)\, dt = \frac{\pi}{2}$ condition.

The NOT gate pulse represents a series of infinitesimal rotations about the x-axis and in order to give the correct NOT gate effect, we need to normalize the pulse by $\int_{-\infty}^{\infty} \theta_G(t)\, dt = \frac{\pi}{2}$. The same form can be applied to a one qubit Hadamard

$$\Omega = \mathscr{H} = \frac{1}{\sqrt{2}}\begin{pmatrix} 1 & 1 \\ 1 & -1 \end{pmatrix} = \frac{\sigma_1 + \sigma_3}{\sqrt{2}}, \tag{32}$$

which is a spinor rotation about the $(\hat{x} + \hat{z})/\sqrt{2}$ axis by π radians.

3.2.2. Bias gates

Application of such a gate pulse does not carry out our objective of achieving a NOT gate, unless we do something to remove the level splitting at least during the action of the pulse. This corresponds to a temporary stoppage of precession. We therefore, introduce a bias pulse which is designed to make the levels degenerate during the gate pulse. The strength of the bias is adjusted by some type of non-intrusive monitoring, or by fore-knowledge of the fixed level splitting, to temporarily establish level degeneracy. During the action of the gate, the levels have to be completely degenerate, otherwise disruptive phases accumulate. Therefore, we use a soft square bias pulse that straddles the time interval of the gate pulse. The soft square bias pulse shape is defined by: $\theta_B(t) \equiv \theta_s(t)/\theta_s(t_0)$, which is

[5] The unitary operator associated with this gate generator is: $U_G(t, t_1) = e^{-\frac{i}{\hbar}\int_{t_1}^{t} V_G(t')dt'}$.

preferred over a square pulse since it has finite derivatives and thus yields smooth variations of power as shown later. The width of the above bias pulse is $\tilde{t}_2 - \tilde{t}_1$, and τ is the thickness of the edges. To be sure that no precession occurs during a gate the time values used in the bias pulses $\tilde{t}_2$ and $\tilde{t}_1$ are taken to be slightly larger and slightly smaller than the gate pulse values t_2 and t_1.

The bias pulse $\theta_B(t)$ is added to the Hamiltonian to create a temporary degeneracy as

$$V_B(t) = \frac{\hbar\,\omega_L}{2}\,\theta_B(t)\,\sigma_3, \tag{33}$$

where the bias normalization is $\int_{-\infty}^{\infty}\theta_B(t)\,dt = 1$. Note θ_B is unitless, whereas θ_G has 1/time units.

Combining these terms we have for a single pulse, with gate and bias

$$H_1(t) = -\frac{\hbar\,\omega_L}{2}\,(1-\theta_B(t))\,\sigma_3 + \hbar\,\theta_G(t)\,\Omega.$$

Here we see that the bias turns off precession and the gate term generates the action of a gate Ω. Without a bias pulse to produce level degeneracy, awkward phases accumulate that are detrimental to clean-acting gates. Aside from intervals when the gate and the bias pulse act, the polarization vector precesses at the Larmor frequency, which is zero for degenerate levels. The bias pulse is simply an action to stop the precession, then the gate pulse rotates the qubit, and subsequently precession is restored once the bias is removed. That process is equivalent to stopping a spinning top, rotate it, and then get it spinning again, which requires some work. As discussed later the power supplied to the system during a gate pulse is determined by

$$\frac{d}{dt}W(t) = \mathrm{Tr}(\rho(t)\,\dot{H}(t)) = +\frac{\hbar\,\omega_L}{2}\,\dot{\theta}_B(t)\,P_z(t) + \hbar\,\dot{\theta}_G(t)\langle\Omega\rangle.$$

The derivative of the Hamiltonian divides into a gate plus a bias term.

3.2.3. Gate and bias cases

In Figs. 3–4, the one-qubit polarization vector motion for a NOT and a Hadamard gate is shown with no dissipation ($\mathcal{L} \to 0$) and with a bias pulse acting during the gate pulse. The detailed case shows that during the NOT pulse one gets the expected change of $P_x \to P_x$; $P_y \to -P_y$; $P_z \to -P_z$. The power supplied to the system during the NOT gate is also displayed separately for the gate power and the bias power. These are explained by the bias power $= (\hbar\,\omega_L/2)\,\dot{\theta}_B(t)P_z(t)$ and the gate power $= \hbar\,\dot{\theta}_G\,P_x(t)$, where the x-polarization is fixed during the NOT gate, but the z-polarization flips. The values of the polarization from the time t_1 when the gate pulse starts to its end at t_2 explain the shapes seen in Fig. 3.

During the Hadamard pulse one gets the expected change of $P_x \to P_z$; $P_y \to -P_y$; $P_z \to P_x$. The power supplied to the system during the Hadamard gate is also displayed separately for the gate power and the bias power. These are explained by the bias power $= P_z(t)\,(\hbar\,\omega_L/2)\,\dot{\theta}_B(t)$ and the gate power $= \hbar\,(P_x(t)+P_z(t))\,\dot{\theta}_G/\sqrt{2}$, where the y-polarization flips during the Hadamard gate, and the z and the x polarization interchange. The values of the polarization during the pulse explain the shapes seen in Fig. 4.

The gate pulses can produce network done on the system. No heat transfer occurs by way of the gate or bias, that exchange arises later from dissipation. After the gate pulses are complete, the precession continues about the $\hat{z}$ axis.

Another case of a Hadamard gate is shown in Fig. 5. In this case, the Hamiltonian is smoothly rotated from $\hat{z}$ to $\hat{x}$ during the Hadamard gate pulse. This Hamiltonian rotation, which is equivalent to rotating a level splitting magnetic field from the z to the x direction, is accomplished by setting:

$$H_1(t) \to -\frac{\hbar\,\omega_L}{2}\,(1-\theta_B(t))(\eta(t_0-t)\,\sigma_3 + \eta(t-t_0)\,\sigma_1) + \hbar\,\theta_G(t)\,\mathcal{H}, \tag{34}$$

$$\eta(t) \equiv \frac{1+\mathrm{Erf}(t/a)}{2}.$$

Here η is a smooth step function of width a. As a result the precession which started around the $\hat{z}$ continues about the $\hat{x}$ axis after the Hadamard gate pulse as shown in Fig. 5.

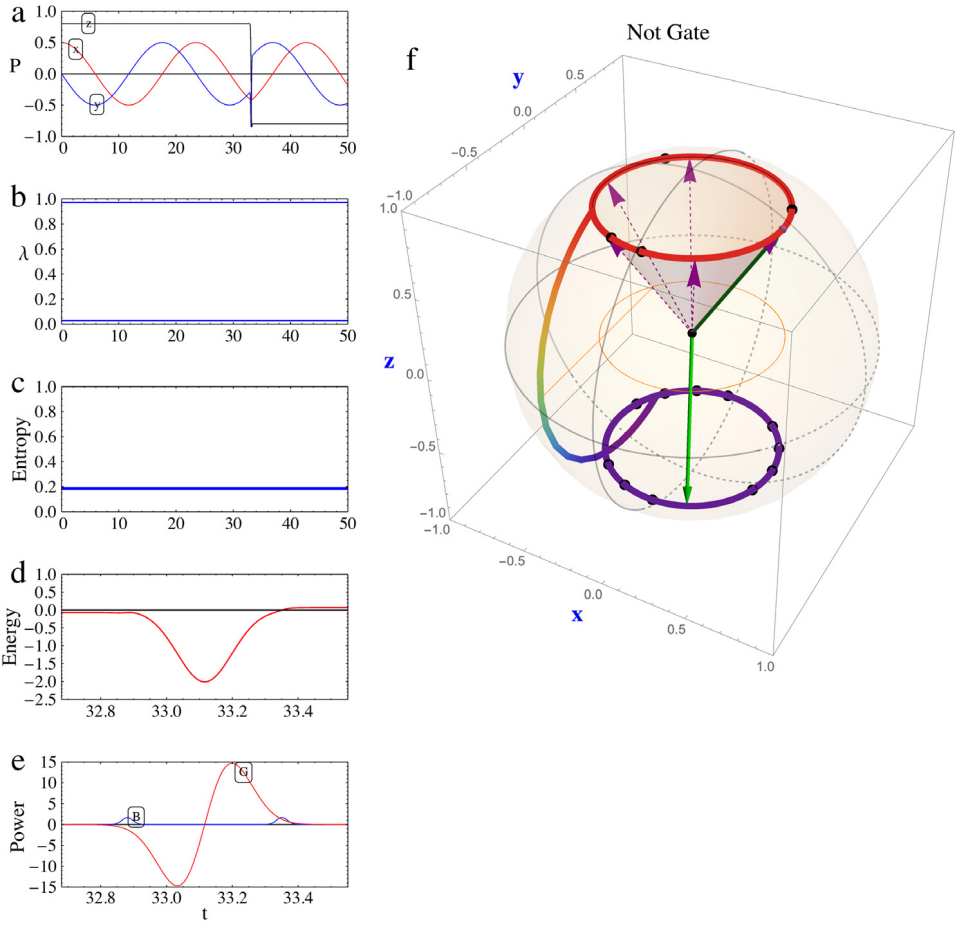

Fig. 3. Polarization vector trajectory for unitary Not Gate with level splitting and bias. Dissipation is off $\mathcal{L} \to 0$. (a) Changes in polarization with time, $P_x \to P_x$, $P_y \to -P_y$, $P_z \to -P_z$ during Not Gate pulse; (b) the two (fixed) eigenvalues λ of $\rho(t)$; (c) the fixed entropy; (d) the energy versus time; (e) Power by gate (G) and bias (B) (heat rate is zero). Here P_y is negative during the gate; and (f) precession about positive $\hat{z}$ is moved to $-\hat{z}$ axis by NOT gate. The dots indicate equal time interval locations of the polarization vector.

3.2.4. Gate pulses and instantaneous gates

To fully replicate the results obtained when a set of instantaneous gates act, as in a QC algorithm, it is necessary to invoke additional steps. One possible step is to apply a bias pulse over the full set of gate pulses, thereby making the qubits degenerate during a QC action, including final measurements. Another way, which we prefer, is to let the precession continue between gate pulses, which means that each gate acts with an associated bias pulse, as illustrated earlier. Then one needs to design the gate pulses and associated measurements to act at appropriate times to replicate the standard description of instantaneous gates. For example, we define a delay time T_D as an integer n_D multiple of the Larmor period T_L. The first gate starts at a time $t_1^{(1)} \equiv T_D = n_D T_L$. The first pulse ends at a time $t_2^{(1)} \equiv t_1^{(1)} + \tau$. The next gate starts at a time $t_1^{(2)} \equiv t_1^{(1)} + T_D$ and ends at a time $t_2^{(2)} \equiv t_1^{(2)} + \tau$. This setup repeats for N_G gates and yields the final time that we use to define the completion of the QC process as $T_f \equiv N_G T_D + \tau = N_G T_D + t_2 - t_1$. At the time T_f the action of the gates is complete and the corresponding density matrix $\rho(T_f)$ is the same as the instantaneous, static gate result $U_G \rho(0) U_G^\dagger$,

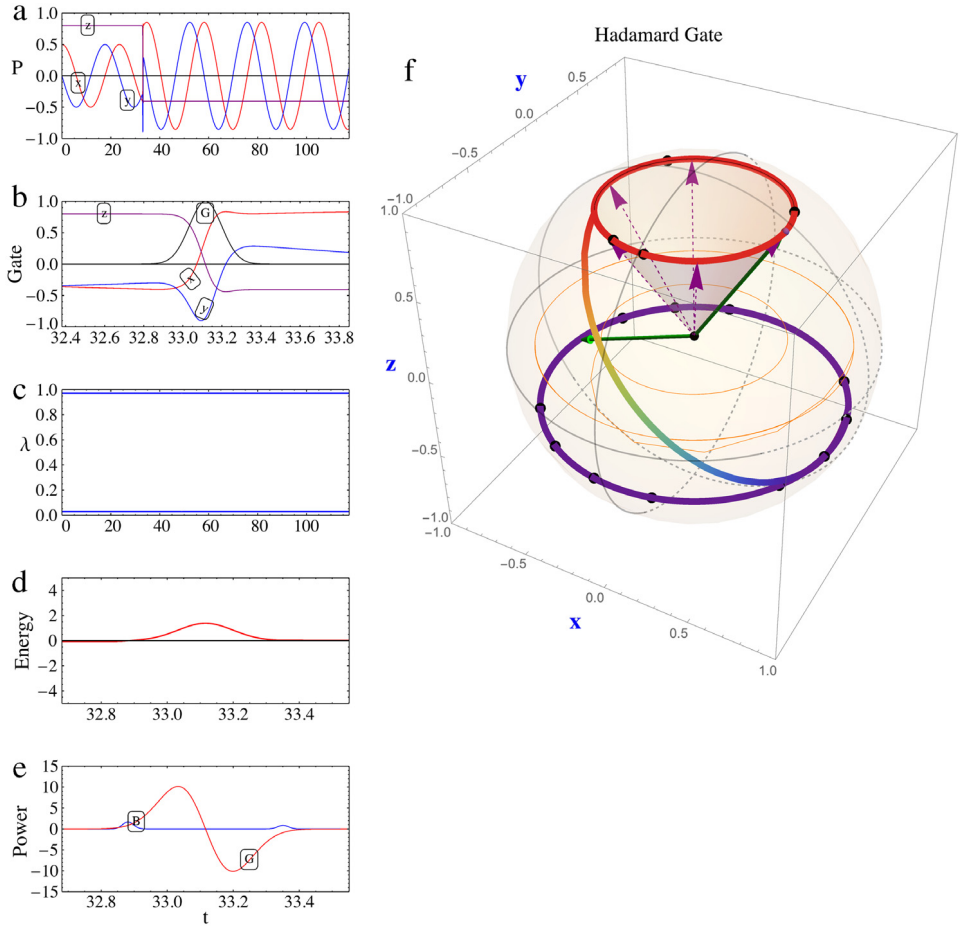

Fig. 4. Polarization vector trajectory for a unitary Hadamard gate with level splitting and bias. Dissipation is off $\mathcal{L} \to 0$. (a) Polarization versus time; (b) Polarization evolution $P_x \to P_z, P_y \to -P_y, P_z \to P_x$ during Hadamard gate pulse(G) when gate starts $t_1 = 32.9$ ns, $(Px, Py, Pz) = (-0.402, -0.301, 0.798)$; (c) the two (fixed) eigenvalues λ_1, λ_2 of $\rho(t)$; (d) the energy versus time; (e) Power by gate (G) and bias (B) (heat rate is zero); and (f) Polarization vector trajectory, precession about positive $\hat{z}$ continues after polarization is moved as shown by Hadamard gate.

where U_G is a product of the N_G gate operators. The general result for the final time is

$$T_f = N_G\, T_D + \tau + n_T\, T_L.$$

For example, consider a three gate case for one qubit $U_G \equiv \mathcal{H} \cdot \sigma_x \cdot \mathcal{H} \equiv \sigma_z$, which is a three gate $N_G = 3$ Hadamard-Not-Hadamard sequence. This case is illustrated in Fig. 6. At the first stage before the gate acts, the polarization vector precesses about the z-axis, then the Hadamard acts at time $t_1^{(1)}$ and the polarization path moves rapidly to the second lower precession circle at time $t_2^{(1)}$. After a few precessions, the Not gate brings the path to the negative z region at time $t_2^{(2)}$. Finally, the final Hadamard lifts the path back up to the original precession cone, but with a phase change. The final result at time $T_f = 3\,T_D + t_2 - t_1$ is obtained by the transformation $P_x \to -P_x, P_y \to -P_y, P_z \to P_z$, which is, as it should be, equivalent to the action of a single σ_z gate. The projected version also shown in Fig. 7 displays this process and the finite time dynamic gate actions.

This process can be implemented for any set of gate pulses and can be generalized to multi-qubit/qutrit cases. Thus the pulsed gate approach can replicate the standard instantaneous static

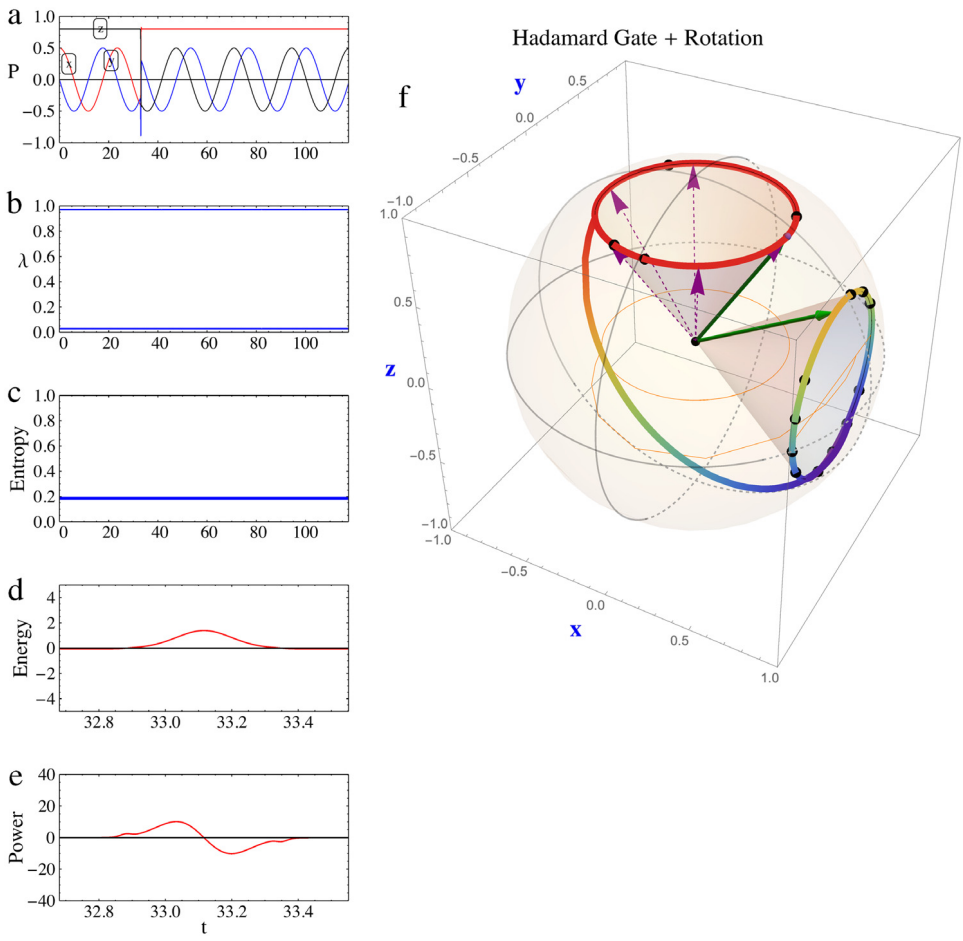

Fig. 5. Polarization vector trajectory for unitary Hadamard Gate plus bias and with $\mathcal{L}$ off. The precession axis is changed from the $\hat{z}$ to the $\hat{x}$ axis during the gate pulse. (a) Changes in polarization $P_x \to P_x$, $P_y \to -P_y$, $P_z \to -P_z$ during Hadamard gate pulse; (b) the two (fixed) eigenvalues λ_1, λ_2 of $\rho(t)$; (c) the fixed entropy; (d) the energy versus time changes due to gate, bias and Hamiltonian axis rotation; (e) Power by gate, bias and Hamiltonian rotation (heat rate is zero); (f) precession starts about $\hat{z}$ axis and continues about $\hat{x}$ axis after polarization is moved as shown by Hadamard gate. The dots indicate equal time interval locations of the polarization vector.

gate description by carefully designing the timing of the gates on the Larmor precession time grid. This requires examining or measuring the gates at the selected time T_f. If the Larmor period T_L varies in time, this procedure can be generalized.

For a sequence of N_G gates

$$H(t) = \sum_{i=1}^{N_G} H_1(t - t_i^0)$$
$$= \sum_{i=1}^{N_G} -\hbar \frac{\omega_L}{2} (1 - \theta_B(t - t_i^0))\sigma_3 + \theta(t - t_i^0)\, \Omega_i \tag{35}$$

where Ω_i is the ith gate acting at the time centered at $t_0 + t_i^0$. This can generate a chain of gates.

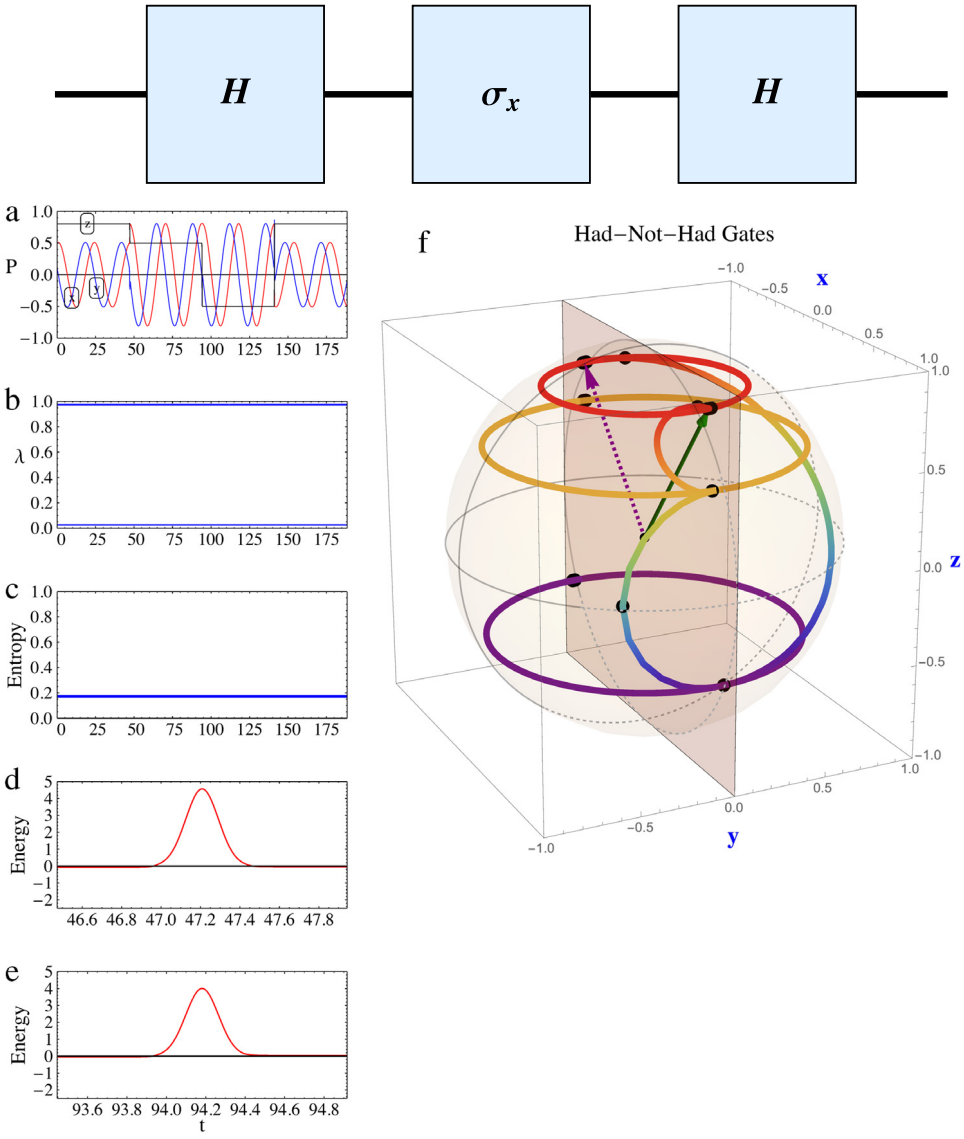

Fig. 6. Polarization for Hadamard–Not–Hadamard pulse gates. (a) Polarization vectors, (b) Eigenvalues, (c) Entropy, (d) Energy of first pulse, (e) Energy of second pulse, all versus time. Then in (f) Trajectories and initial and final polarization vectors, along with the three rapid gate pulses. The initial polarization vector (solid green arrow) $(P_x, P_y, P_z) = (0.5, 0.1, 0.8)$ and final polarization vector (dashed purple arrow) $(-0.5, -0.1, 0.8)$ are seen to give the expected σ_z gate result.

We conclude that one can replicate the action of instantaneous static gates, which is central to the usual description of QC algorithms, by including a bias pulse during the gate action, and by applying the gates on the Larmor period time-grid.

3.3. Schrödinger, Heisenberg, Dirac (interaction) and rotating frame pictures

In our treatment, we use the Schrödinger picture for the density matrix, so that all aspects of the dynamics are described by the density matrix through its polarization and spin correlation

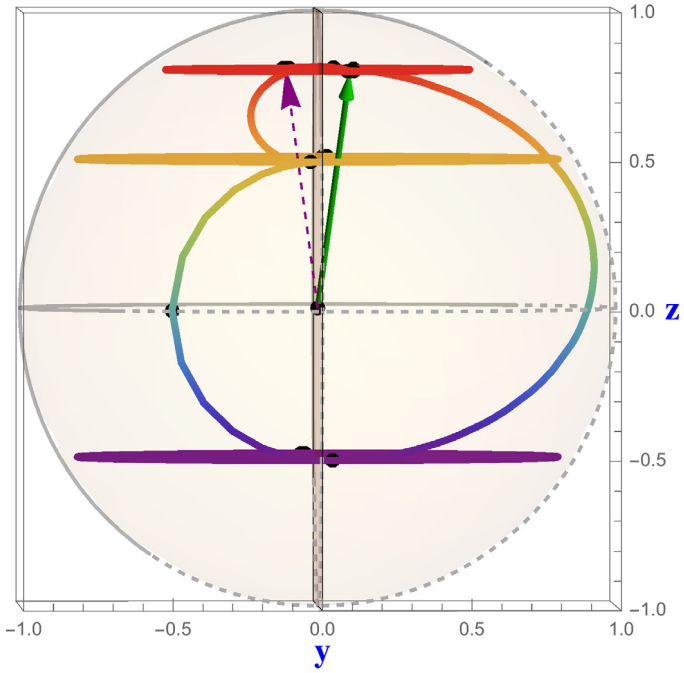

Fig. 7. Polarization trajectories for Hadamard–Not–Hadamard pulse gates projected onto the y–z plane. The first Hadamard downward pulse is seen with the next Not downward pulse, and then the final upward Hadamard pulse. In this example, the initial polarization vector (solid green arrow) $(P_x, P_y, P_z) = (0.5, 0.1, 0.8)$ and final polarization vector (dashed purple arrow) $(-0.5, -0.1, 0.8)$ are seen projected onto the y–z plane.

observables. Other choices are to either use the Heisenberg picture, where the time development is incorporated into the Hermitian operators, or use the Dirac or Interaction picture, wherein the operators evolve in time with the "free" Hamiltonian $H_0(t)$. Then the Dirac picture density matrix $\tilde{\rho}(t) = e^{+iH_0(t)\,t/\hbar}\,\rho(t)\,e^{-iH_0(t)\,t/\hbar}$ evolves as:

$$\frac{d\tilde{\rho}(t)}{dt} = -\frac{i}{\hbar}\Big[\tilde{V}(t), \tilde{\rho}(t)\Big] + \tilde{\mathscr{L}}, \tag{36}$$

where the tilde denotes interaction picture operators. For the choice of $H_0(t) = -\hbar\omega_L\,\sigma_3/2$, going to the Dirac picture is simply going to a frame rotating about the z-axis in which frame the Larmor precession vanishes. That is called the rotating frame. Since we include gates into $V(t)$ and hence $\tilde{V}(t)$, the gate bias pulse that we introduce in the Schrödinger picture, corresponds to a rotating frame that stops rotating during the action of a gate.

There are advantages offered by each of these choices. We stick with the Schrödinger description because it most clearly reveals the full dynamics by viewing the time evolution of the spin observables.

4. The master equation model

The master equation for the time evolution of the system's density matrix is now presented. We seek a simple model that incorporates the main features of qubit dynamics for a quantum computer. These main features include seeing how the dynamics evolve under the action of gates and the role of both closed system dynamics and of open system decoherence, dissipation and the system's approach to equilibrium. From the density matrix we can determine a variety of observables, such as the polarization vector, the power and heat rates, the purity, fidelity, and entropy all as a function of time.

4.1. Definition of the model master equation

To the unitary evolution, we now add a term $\mathscr{L}(t)$ which is required to be Hermitian and traceless so that the density matrix $\rho(t)$ maintains its Hermiticity and trace one properties. In addition, $\mathscr{L}(t)$ has to keep $\rho(t)$ positive definite. To identify explicit physical effects, we separate $\mathscr{L}(t)$ into three terms:

$$\begin{aligned}
\frac{d\rho}{dt} &= -\frac{i}{\hbar}\Big[H(t),\,\rho(t)\Big] + \mathscr{L} \qquad (37)\\
\mathscr{L} &= \mathscr{L}_1 + \mathscr{L}_2 + \mathscr{L}_3\\
\mathscr{L}_1 &= \Gamma\Big\{L(t)\,\rho(t)\,L^\dagger(t) - \frac{L^\dagger(t)L(t)\,\rho(t) + \rho(t)\,L^\dagger(t)L(t)}{2}\Big\}, \quad \text{Lindblad}\\
\mathscr{L}_2 &= \gamma_2\,\rho(t)(\tilde{S} - \langle\tilde{S}\rangle) - \gamma_2\,\beta_2(t)\left\{\frac{\rho(t)H(t) + H(t)\rho(t)}{2} - \rho(t)\langle H(t)\rangle\right\} \quad \text{Beretta}\\
\mathscr{L}_3 &= \gamma_3\,\rho(t)(\tilde{S} - \langle\tilde{S}\rangle) - \gamma_3\,\boldsymbol{\beta_3(t)}\left\{\frac{\rho(t)H(t) + H(t)\rho(t)}{2} - \rho(t)\langle H(t)\rangle\right\}, \quad \text{Bath}
\end{aligned}$$

the operator $\tilde{S} \equiv -\log_e \rho(t)$, involves a base e logarithm to assure that a Gibbs density matrix is obtained in equilibrium (see later). The QC entropy is defined with a base 2 operator $\hat{S} = -\log_2 \rho(t)$ with entropy equal to $\langle S\rangle = \langle\hat{S}\rangle = -\mathrm{Tr}[\rho(t)\,\log_2\rho(t)]$. The conversion factor is $\tilde{S} \equiv \log_e(2)\,\hat{S}$ and $\langle\tilde{S}\rangle \equiv \log_e(2)\,\langle\hat{S}\rangle$, with $\log_e(2) = 0.693147$. The level splitting, gates and bias pulses are included in $H(t)$. The state dependent, and hence time dependent, functions $\beta_2(t)$, $\boldsymbol{\beta_3(t)}$ will be defined later.

When we discuss equilibrium, a form that combines the Beretta and Bath terms $\mathscr{L}_{2\,3}(t)$ is used:

$$\mathscr{L}_{2\,3}(t) = \gamma_{23}\,\rho(t)(\tilde{S} - \langle\tilde{S}\rangle) - \gamma_{23}\,\beta_{23}(t)\left\{\frac{\rho(t)H(t) + H(t)\rho(t)}{2} - \rho(t)\langle H(t)\rangle\right\}, \qquad (38)$$

with $\gamma_{23} \equiv \gamma_2 + \gamma_3$, and $\beta_{23}(t) \equiv \frac{\gamma_2\beta_2(t) + \gamma_3\boldsymbol{\beta_3(t)}}{\gamma_{23}}$.

The $\mathscr{L}_1$ is of Lindblad [12] form, where the $L(t)$ are time-dependent Lindblad spin-space operators, which we will represent later as pulses. The most important properties of the $\mathscr{L}_1 \cdots \mathscr{L}_3$ operators are that they are Hermitian and traceless, which means that as the density matrix evolves in time, it remains Hermitian and of unit trace. They also have the property of maintaining the positive definite property of the density matrix. Note Γ sets the rate of the Lindblad contribution $\mathscr{L}_1$, in inverse time units. In our heuristic master equation, we use the Lindblad form to describe the impact of external noise on the system, where we represent the noise as random pulses. In addition, we also use the Lindblad form to describe dissipative/friction effects on the quantum gates, by having the Lindblad pulses coincide with the action time of the gate pulses. We also show later that a strong Lindblad pulse can represent a quantum measurement.

The $\mathscr{L}_2$, term is the Beretta [15–17] contribution, which describes a closed system. The closed system involves no heat transfer, with motion along a path of increasing entropy, as occurs for example with a non-ideal gas in an insulated container. This is accomplished by a state dependent $\beta_2(t)$ that is presented later. Note γ_2, sets the strength of the Beretta contribution $\mathscr{L}_2$, in inverse time units as a fraction of the Larmor angular frequency.

In one simple version of the Bath contribution [18,19] $\mathscr{L}_3$, the Bath temperature T in Kelvin stipulates a fixed value of $\boldsymbol{\beta_3(t)} \to \beta_3 \equiv 1/(k_B\,T)$, where k_B is the Boltzmann constant (86.17 μeV/K). A more general $\mathscr{L}_3$ Bath contribution, based on a general theory [15,16,25] of thermodynamics,[6] defines a state dependent $\boldsymbol{\beta_3(t)}$ by using a fixed temperature T_Q to specify a fixed $\dot{Q}(t)/\dot{S}(t)$ ratio (see later). Note γ_3 sets the strength of the Bath contribution $\mathscr{L}_3$, in inverse time units as a fraction of the Larmor angular frequency.

In Table 2, typical values of ω_L, Γ, γ_2, γ_3, β_3 used in our test cases are shown; these parameters are selected to focus on the role of each term. Realistic values can be invoked for various experimental conditions.

[6] The author gratefully thanks one Reviewer for pointing out this very significant improvement.

Table 2
Test master equation parameters.

Name	Value	Units
ω_L	0.2675	GHz
Γ	0.00213	GHz
γ_2	0.0426	GHz
γ_3	0.0852	GHz
β_3	0.000425	$1/\mu$eV

4.2. Some general properties of the master equation

4.2.1. Power and heat rate evolution

The various terms in the master equation play different roles in the dynamics. To examine those differing roles consider the energy of the system and its rate of change. With our Hamiltonian $H(t)$ and a density matrix $\rho(t)$, we form the ensemble average

$$E(t) = \langle H(t)\rangle \equiv \mathrm{Tr}[H(t)\,\rho(t)].$$

Taking the time derivative, we obtain

$$\begin{aligned} \frac{dE(t)}{dt} &= \mathrm{Tr}\Big[\rho(t)\,\frac{d}{dt}H(t)\Big] + \mathrm{Tr}\Big[H(t)\,\frac{d}{dt}\rho(t)\Big] \\ &= \frac{d}{dt}W(t) + \frac{d}{dt}Q(t) \\ \frac{d}{dt}W(t) &= \mathrm{Tr}[\rho(t)\,\dot{H}(t)] \\ \frac{d}{dt}Q(t) &= \mathrm{Tr}[H(t)\,\dot{\rho}(t)]. \end{aligned} \tag{39}$$

We identify the term $\frac{dQ(t)}{dt}$ as the energy transfer rate and $\frac{dW(t)}{dt}$ as the work per time or power, with the convention that $Q(t) > 0$ indicates heat transferred into the system, and $W(t) >$ indicates work done on the system. The time dependence of the density matrix is given by the unitary evolution plus the $\mathscr{L}$ terms of Eq. (37).

Now consider just the power term. Since $\frac{dH(t)}{dt}$ is nonzero when gate pulses are active, power is invoked in the system only via the time derivatives of the gate and bias pulses (and by any temporal changes in the level splitting).

The energy transfer rate $\frac{dQ(t)}{dt}$ can now be examined using the dynamic evolution

$$\begin{aligned} \mathrm{Tr}\Big[H(t)\,\frac{d\rho(t)}{dt}\Big] &= \mathrm{Tr}\Big[H(t)\Big\{-\frac{i}{\hbar}[\rho(t), H(t)] + \mathcal{L}\Big\}\Big] \\ &= \mathrm{Tr}[H(t)\,\mathcal{L}]. \end{aligned} \tag{40}$$

Using the permutation invariance of the trace, the unitary evolution part does not contribute to energy transfer. Heat arises from the Lindblad and Bath terms. We will now see: (1) how the closed system (Beretta term) does not generate energy transfer; it does increase entropy; and (2) the Bath term involves heat and associated entropy transfer.

The Lindblad term generates energy transfer (heat) according to[7]:

$$\frac{dQ}{dt} = \Gamma\,\mathrm{Tr}\Big[H(t)\Big\{L(t)\,\rho(t)\,L^\dagger(t) - \frac{L^\dagger(t)L(t)\,\rho(t) + \rho(t)\,L^\dagger(t)L(t)}{2}\Big\}\Big]$$

The Beretta term heat transfer equation is:

$$\frac{dQ}{dt} = \gamma_2\,\mathrm{Tr}\Big[H(t)\Big[\rho(t)\,(\tilde{S} - \langle\tilde{S}\rangle) - \beta_2(t)\Big\{\frac{\rho(t)H(t) + H(t)\rho(t)}{2} - \rho(t)\langle H(t)\rangle\Big\}\Big]\Big]$$

[7] Note that if $L(t)$ commutes with $H(t)$, the heat transfer vanishes.

$$= \gamma_2 \left\{ (\langle H(t)\tilde{S}\rangle - \langle H(t)\rangle\langle\tilde{S}\rangle) - \beta_2(t)(\langle H^2(t)\rangle - \langle H(t)\rangle^2) \right\}$$
$$= \gamma_2 \left\{ \langle \Delta E\ \Delta\tilde{S}\rangle - \beta_2(t)\langle \Delta E\ \Delta E\rangle \right\}, \tag{41}$$

where we have defined

$$\begin{aligned}
\langle \Delta E\ \Delta E\rangle &\equiv \langle H^2(t)\rangle - \langle H(t)\rangle^2 = \langle (H - \langle H\rangle)^2\rangle \\
\langle H^2(t)\rangle &\equiv \mathrm{Tr}[\rho(t)\,H(t)\,H(t)] \qquad \langle H(t)\rangle \equiv \mathrm{Tr}[\rho(t)\,H(t)] \\
\langle \Delta E\ \Delta\tilde{S}\rangle &\equiv \langle H(t)\tilde{S}\rangle - \langle H(t)\rangle\langle\tilde{S}\rangle \\
&= \langle (H - \langle H\rangle)(\tilde{S} - \langle\tilde{S}\rangle)\rangle \\
\langle H(t)\tilde{S}\rangle &\equiv \mathrm{Tr}[\rho(t)\,H(t)\tilde{S}] \qquad\qquad \langle\tilde{S}\rangle \equiv \mathrm{Tr}[\rho(t)\,\tilde{S}] \\
\tilde{S} &\equiv -\log_e \rho(t).
\end{aligned} \tag{42}$$

The major feature of Beretta's $\mathcal{L}_2$ contribution is a state and hence time-dependent $\beta_2(t)$

$$\begin{aligned}
\beta_2(t) &\equiv \frac{\langle \Delta E\ \Delta\tilde{S}\rangle}{\langle \Delta E\ \Delta E\rangle} \\
&= \frac{\langle H(t)\tilde{S}\rangle - \langle H(t)\rangle\langle\tilde{S}\rangle}{\langle H^2(t)\rangle - \langle H(t)\rangle\langle H(t)\rangle} \\
&= \frac{\langle (H - \langle H\rangle)(\tilde{S} - \langle\tilde{S}\rangle)\rangle}{\langle (H - \langle H\rangle)^2\rangle},
\end{aligned} \tag{43}$$

defined so that the system is closed and energy is not transferred to or from the system, $\frac{dQ}{dt} = 0$. This choice also makes the closed system follow a path of increasing entropy (see later). That increase of entropy for a closed system signifies that the closed system is dynamically constrained to reorder itself to maximize its entropy. Here $\beta_2(t)$ has a highly nonlinear dependence on the density matrix. For a one qubit system, $\beta_2(t)$ is of rather simple form

$$\beta_2(t) = 2\,\frac{1 - \mathbf{P}(t)^2}{1 - P_z(t)^2}\,\frac{P_z(t)}{\mathbf{P}(t)}\,\frac{\mathrm{arctanh}(\mathbf{P}(t))}{\hbar\,\omega_L}, \tag{44}$$

for an equilibrium Gibbs density matrix with fixed z and zero x and y polarization, this reduces to $\beta_2(t) = 2\ \mathrm{arctanh}(P_z)/(\hbar\,\omega_L) = \frac{\log_e(1+P_z)}{\log_e(1-P_z)}/(\hbar\,\omega_L)$.

The Bath term $\mathcal{L}_3$ does generate heat:

$$\begin{aligned}
\frac{dQ}{dt} &= \gamma_3\,\mathrm{Tr}\Big[(H(t))\,\rho(t)\left\{ (\tilde{S} - \langle\tilde{S}\rangle) - \boldsymbol{\beta_3(t)}(H(t) - \langle H(t)\rangle) \right\} \Big] \\
&= \gamma_3 \left\{ (\langle H(t)\tilde{S}\rangle - \langle H(t)\rangle\langle\tilde{S}\rangle) - \boldsymbol{\beta_3(t)}(\langle H^2(t)\rangle - \langle H(t)\rangle\langle H(t)\rangle) \right\} \\
&= \gamma_3 \left\{ \langle \Delta E\ \Delta\tilde{S}\rangle - \boldsymbol{\beta_3(t)}(\langle \Delta E\ \Delta E\rangle) \right\}
\end{aligned} \tag{45}$$

where the Korsch [18,19] option sets $\boldsymbol{\beta_3(t)} \to \beta_3 = 1/(k_B\,T)$ to a constant, where T is a specified bath temperature. Entropy is changed by the bath term. A better choice for $\boldsymbol{\beta_3(t)}$ involves the entropy evolution, which is discussed next.

4.2.2. Entropy evolution

Let us now consider the time evolution of the base 2 entropy Eq. (22). Eq. (24) gives the time derivative of the entropy as $\frac{dS}{dt} = -\mathrm{Tr}[\log_2(\rho(t))\,\frac{d\rho(t)}{dt}]$. Inserting the time derivative from Eq. (37), we again get no change from the unitary term, just from the dissipative $\mathcal{L}$ terms:

$$\begin{aligned}
\frac{dS}{dt} &= -\mathrm{Tr}\Big[\log_2(\rho(t))\,\frac{d\rho(t)}{dt} \Big] \\
&= -\mathrm{Tr}[\log_2(\rho(t))\,\mathscr{L}].
\end{aligned} \tag{46}$$

This is a general result for n_q qubits.

Note that the Lindblad term generates a change in entropy according to:

$$\begin{aligned}\frac{dS}{dt} &= -\Gamma\,\mathrm{Tr}\Big[\log_2(\rho(t))\,\Big\{L(t)\,\rho(t)\,L^\dagger(t) - \frac{L^\dagger(t)L(t)\,\rho(t) + \rho(t)\,L^\dagger(t)L(t)}{2}\Big\}\Big]\\ &= -\Gamma\,\mathrm{Tr}\Big[\log_2(\rho(t))\,\{L(t)\,\rho(t)\,L^\dagger(t) - \rho(t)L^\dagger(t)L(t)\,\}\Big]\\ &= -\Gamma\,\mathrm{Tr}\Big[\log_2(\rho(t))\,[L(t),\,\rho(t)L^\dagger(t)]\Big]. \end{aligned} \tag{47}$$

For the Beretta (closed system) $\mathcal{L}_2$ and the Bath $\mathcal{L}_3$ terms, entropy changes according to:

$$\frac{dS}{dt} = -\gamma_2\,\mathrm{Tr}\Big[\log_2(\rho(t))\,\rho(t)\,\Big\{(\tilde{S} - \langle\tilde{S}\rangle) - \beta_2(t)(H(t) - \langle H(t)\rangle)\Big\}\Big] \tag{48}$$

$$\frac{dS}{dt} = -\gamma_3\,\mathrm{Tr}\Big[\log_2(\rho(t))\,\rho(t)\,\Big\{(\tilde{S} - \langle\tilde{S}\rangle) - \boldsymbol{\beta_3(t)}(H(t) - \langle H(t)\rangle)\Big\}\Big].$$

For the Beretta closed system case, with $\langle\Delta\tilde{S}\,\Delta\tilde{S}\rangle \equiv \langle\tilde{S}^2\rangle - \langle\tilde{S}\rangle^2 = \langle(\tilde{S} - \langle\tilde{S}\rangle)^2\rangle$:

$$\begin{aligned}\frac{dS}{dt} &= +\frac{\gamma_2}{\log_e(2)}\Big[(\langle\tilde{S}^2\rangle - \langle\tilde{S}\rangle^2) - \beta_2(t)(\langle H(t)\tilde{S}\rangle - \langle H(t)\rangle\langle\tilde{S}\rangle)\Big]\\ &= +\frac{\gamma_2}{\log_e(2)}\Big[\langle\Delta\tilde{S}\,\Delta\tilde{S}\rangle - \beta_2(t)\langle\Delta E\,\Delta\tilde{S}\rangle\Big]\\ &= +\frac{\gamma_2}{\log_e(2)}\Big[\langle\Delta\tilde{S}\,\Delta\tilde{S}\rangle\langle\Delta E\,\Delta E\rangle - \langle\Delta E\,\Delta\tilde{S}\rangle^2\Big]/\langle\Delta E\,\Delta E\rangle. \end{aligned} \tag{49}$$

Note that entropy increases for the Beretta term $\frac{dS}{dt} \geq 0$, since $\langle\Delta\tilde{S}\,\Delta\tilde{S}\rangle\,\langle\Delta E\,\Delta E\rangle \geq \langle\Delta E\,\Delta\tilde{S}\rangle^2$.

For the Bath term, when we switch to a base "e" entropy $\tilde{S}$,

$$\frac{d\tilde{S}}{dt} = +\gamma_3\Big[\langle\Delta\tilde{S}\,\Delta\tilde{S}\rangle - \boldsymbol{\beta_3(t)}\langle\Delta E\,\Delta\tilde{S}\rangle\Big]. \tag{50}$$

Forming the energy rate to entropy rate ratio and setting it equal to a fixed quantity $k_B T_Q$, we obtain the condition $k_B T_Q = dQ/d\tilde{S} = \dot{Q}/\dot{\tilde{S}}$

$$\frac{\dot{Q}}{\dot{\tilde{S}}} = \frac{\langle\Delta E\,\Delta\tilde{S}\rangle - \boldsymbol{\beta_3(t)}\langle\Delta E\,\Delta E\rangle}{\langle\Delta\tilde{S}\,\Delta\tilde{S}\rangle - \boldsymbol{\beta_3(t)}\langle\Delta E\,\Delta\tilde{S}\rangle} = k_B\,T_Q, \tag{51}$$

which yields an expression for the state dependence of $\boldsymbol{\beta_3(t)}$:

$$\boldsymbol{\beta_3(t)} = \frac{\langle\Delta E\,\Delta\tilde{S}\rangle - k_B T_Q\,\langle\Delta\tilde{S}\,\Delta\tilde{S}\rangle}{\langle\Delta E\,\Delta E\rangle - k_B T_Q\,\langle\Delta E\,\Delta\tilde{S}\rangle}. \tag{52}$$

For the equilibrium (Gibbs density matrix) limit, which occurs at final time t_f, $\boldsymbol{\beta_3(t_f)} \to \beta_3 = \frac{1}{k_B T}$, where T is the specified Bath (Gibbs) temperature. In equilibrium, the polarization vector is in the z-direction since $H[t_f] = H_0 \equiv -\frac{1}{2}\,\hbar\,\omega_L\,\sigma_z$. The difference between the two Bath versions for one qubit evolution will be explored later.

4.2.3. Purity evolution

For a one qubit system, both the entropy and the purity are functions of the length of the polarization vector, with the entropy being zero and the purity being one on the Bloch sphere. For polarization vectors inside the Bloch sphere, the entropy is increased and the purity decreased. Note that $1 - \mathcal{P}(t)$ plays a role parallel to entropy. Consider the change in Purity (denoted by the symbol $\mathcal{P}$), where

$$\mathcal{P}(t) \equiv \mathrm{Tr}[\rho(t)\,\rho(t)],$$

and the rate of change of this purity is given by

$$\frac{d\mathcal{P}(t)}{dt} = 2\,\mathrm{Tr}\Big[\rho(t)\,\frac{d\rho(t)}{dt}\Big].$$

Using Eq. (25), we find that the purity is unchanged by the unitary term, but is altered, mainly diminished, by the Lindblad term:

$$\begin{aligned}\frac{d\mathcal{P}(t)}{dt} &= 2\,\mathrm{Tr}\Big[\rho(t)\,\mathscr{L}_1\Big] \\ &= 2\,\Gamma\,\mathrm{Tr}\Big[\rho(t)\,\Big\{L(t)\,\rho(t)\,L^\dagger(t) - \frac{L^\dagger(t)L(t)\,\rho(t) + \rho(t)\,L^\dagger(t)L(t)}{2}\Big\}\Big] \\ &= 2\,\Gamma\,\mathrm{Tr}\Big[\rho(t)\,\Big\{L(t)\,\rho(t)\,L^\dagger(t) - L^\dagger(t)L(t)\,\rho(t)\Big\}\Big] \\ &= 2\,\Gamma\,\mathrm{Tr}\Big[\rho(t)\,[L(t),\,\rho(t)\,L^\dagger(t)]\Big]. \end{aligned} \tag{53}$$

The trace property $\mathrm{Tr}[AB] = \mathrm{Tr}[BA]$ was again invoked to deduce that $\mathrm{Tr}\Big[\rho(t)\,[H(t),\,\rho(t)]\Big] \equiv 0$.

4.2.4. Temperature

Temperature is a basic quantity in equilibrium thermodynamics. It is not clear if any such concept can be applied to non-equilibrium systems. Nevertheless, it is tempting to invoke a "temperature" quantity for dynamic systems, albeit with caution. In that spirit, we note that the inverse temperature β does apply to the equilibrium Gibbs state. Two possible definitions of temperature for non-equilibrium cases are based on (1) the level occupation probability ratios or (2) the ratio of the energy change and the entropy change $k_B T = dQ/d\tilde{S} = \dot{Q}/\dot{\tilde{S}}$.

The simplest case (1) occurs for a diagonal Hamiltonian (for us that occurs away from gate pulses), the ensemble average energy is:

$$\langle H(t)\rangle = \mathrm{Tr}[H(t)\,\rho(t)] = -\frac{\hbar\omega_L}{4}\mathrm{Tr}[\sigma_3\,P_z\sigma_3] = -\frac{\hbar\omega_L}{2}P_z = \epsilon_1\,\rho_{11} + \epsilon_2\,\rho_{22}, \tag{54}$$

where $\epsilon_1 = -\hbar\omega_L/2$, $\epsilon_2 = \hbar\omega_L/2$, $\rho_{11} = (1+P_z)/2$ and $\rho_{22} = (1-P_z)/2$. Here we see the connection between temperature and the z-polarization, and that the level occupation probabilities are $n_1 = \rho_{11}$ and $n_2 = \rho_{22}$.

When the gates are acting, we need to include off-diagonal terms in $H(t)$. So we introduce the unitary operator $\tilde{U}(t)$ that diagonalizes $H(t) = \tilde{U}^\dagger(t)\,H_d(t)\,\tilde{U}(t)$

$$\langle H(t)\rangle = \mathrm{Tr}[H(t)\,\rho(t)] = \mathrm{Tr}[H_d(t)\,\tilde{\rho}(t)] = \tilde{\epsilon_1}\,\tilde{\rho}_{11} + \tilde{\epsilon}_2\,\tilde{\rho}_{22}, \tag{55}$$

where $\tilde{\epsilon_1}, \tilde{\epsilon_2}$ are the eigenvalues of $H(t)$ and $\tilde{\rho} \equiv \tilde{U}(t)\rho(t)\tilde{U}^\dagger(t)$. In this way we can define level occupation probabilities including gate pulses: $\tilde{n}_1 = \tilde{\rho}_{11}$ and $\tilde{n}_2 = \tilde{\rho}_{22}$.

Note that for a system described by a Gibbs density matrix, that density matrix commutes with the Hamiltonian. As a consequence, the unitary evolution vanishes. Thus for a Gibbs equilibrium state the Hamiltonian and the density matrix are diagonalized by the same unitary matrix. In addition, for a Hamiltonian of the form $H \propto \sigma_z$, the polarization in the x and y directions vanishes for a Gibbs density matrix, and $P_z = \tanh(\frac{\hbar\omega_L}{2k_BT})$, which relates the z-polarization to the absolute temperature T in a rather complicated way. A simpler form follows.

We use the Gibbs density matrix

$$\rho_G \equiv \frac{e^{-\frac{H(t)}{k_BT}}}{\mathcal{Z}}; \quad \mathcal{Z} \equiv \mathrm{Tr}(e^{-\frac{H(t)}{k_BT}})$$

to define absolute temperature

$$T = \frac{1}{k_B}\frac{\tilde{\epsilon}_2 - \tilde{\epsilon}_1}{\log_e(\frac{\tilde{n}_1}{\tilde{n}_2})}. \tag{56}$$

In the region away from the gate pulses where the Hamiltonian is diagonal, this reduces to

$$T = \frac{\hbar\omega_L}{k_B}\frac{1}{\log_e(\frac{n_1}{n_2})} \tag{57}$$

the above definition is equivalent to $P_z = \tanh(\frac{\hbar\omega_L}{2k_BT})$.

Note the above temperature definition yields a positive absolute temperature for $n_1 \geq n_2$, for larger ground state occupation, but negative absolute temperature for $n_2 > n_1$. This is the well known, negative absolute temperature that appears for a small number of levels that are excited to produce a "level occupation/temperature inversion" [28,29]. For us that appears when the z-polarization flips sign.

Case (2) $k_B T = dQ/d\tilde{S} = \dot{Q}/\dot{\tilde{S}}$ can be evaluated from the ratio of the time derivatives of the heat and of the entropy. The result is

$$T = \frac{\hbar\omega_L}{k_B}\frac{\dot{P}_z}{\dot{\mathbf{P}}}\frac{1}{\log_e(\frac{1+\mathbf{P}}{1-\mathbf{P}})} \quad \underset{P_x=P_y\to 0}{\Longrightarrow} \quad \frac{\hbar\omega_L}{k_B}\frac{1}{\log_e(\frac{1+P_z}{1-P_z})},$$

which reduces to the above case (1) definition when P_x and P_y vanish. Here $\mathbf{P}$ is the length of the polarization vector.

These two thermodynamic definitions can simply be extended to the gate and to non-equilibrium regions by fiat. Non-equilibrium situations occur when P_x and P_y are non-zero. The above two quantities have the units of temperature in all regions, but a clear meaning of temperature applies only for equilibrium. Nevertheless, it is of interest to use T as defined above in non-equilibrium regions where they serve as useful indicia of dynamical changes.

4.3. Lindblad

4.3.1. Comments on positive definite property of Lindblad

An explicit demonstration for one-qubit that the Lindblad term keeps $\rho(t)$ positive definite is obtained by setting $\rho(t) = U_\rho(t)\rho_D(t)U_\rho^\dagger(t)$, where $\rho_D(t)$ is the diagonal matrix $\begin{pmatrix}\lambda_1 & 0\\ 0 & \lambda_2\end{pmatrix}$. It then follows that the commutator term does not alter the eigenvalues and that the Lindblad term keeps the eigenvalues positive and between zero and 1. One finds[8]: $\dot{\lambda}_i(t) = [U_\rho^\dagger(t)\,\mathcal{L}_1\,U_\rho(t)]_{ii}$

$$\frac{d\lambda_1(t)}{dt} = \Gamma|V_{1,2}|^2\,(1-\alpha\,\lambda_1(t)),$$

where $\alpha = (|V_{2,1}|^2 + |V_{1,2}|^2)/|V_{1,2}|^2 > 1$ and $V \equiv U_\rho^\dagger(t)\,L\,U_\rho(t)$. This form shows that the eigenvalues stay within the zero to 1 region.

For a system of $n_q > 1$ qubits, the above generalizes to:

$$\begin{aligned}\frac{d\lambda_i(t)}{dt} &= \Gamma\left[\Big[\sum_s |V_{is}|^2\lambda_s\Big] - (V^\dagger V)_{ii}\lambda_i\right]\\ &= \Gamma\sum_{s\neq i}(|V_{is}|^2\lambda_s - |V_{si}|^2\lambda_i),\end{aligned} \tag{58}$$

where $i = 1\cdots 2^{n_q}$ and the eigenvalues are ordered from the largest to smallest. From this equation, it follows that the largest and smallest eigenvalues stay within the zero to one range if they start in that range and therefore all eigenvalues are within that range. For example, as the largest eigenvalue $\lambda_1 \to 1$, the other eigenvalues approach zero and hence $\frac{d\lambda_1(t)}{dt} = -\Gamma\sum_{s\neq 1}|V_{s1}|^2 \leq 0$. This negative derivative bounces the eigenvalue back into the zero to one range, if it approaches one. When the smallest eigenvalue approaches zero the other eigenvalues are all positive and less than 1, and hence $\frac{d\lambda_{n_q}(t)}{dt} = +\Gamma\sum_{s\neq n_q}|V_{n_q s}|^2\lambda_s \geq 0$. This positive derivative bounces the eigenvalue back into the zero to one range, if it approaches zero. This is a very simple proof that the Lindblad form preserves the positive definite nature of a density matrix.

The same steps using the diagonal density matrix basis apply to the derivative of the entropy:

$$\frac{dS}{dt} = -\Gamma\sum_{si}\log_2\lambda_i\,(|V_{is}|^2\lambda_s - |V_{si}|^2\lambda_i), \tag{59}$$

[8] Note $\frac{d}{dt}(U_\rho\,\rho_D\,U_\rho^\dagger) = U_\rho\,\dot{\rho}_D\,U_\rho^\dagger + \dot{U}_\rho\,\rho_D\,U_\rho^\dagger + U_\rho\,\rho_D\,\dot{U}_\rho^\dagger$ and $U_\rho^\dagger\,\frac{d\rho}{dt}\,U_\rho = \dot{\rho}_D + U_\rho^\dagger\,\dot{U}_\rho\,\rho_D + \rho_D\,\dot{U}_\rho^\dagger\,U_\rho$. For the ith diagonal component the last two terms vanish since $\frac{d}{dt}(U_\rho^\dagger\,U_\rho) = 0$. Thus we arrive at $\dot{\lambda}_i(t) = [U_\rho^\dagger(t)\,\mathcal{L}\,U(t)_\rho]_{ii}$.

and to the purity

$$\frac{d\mathcal{P}(t)}{dt} = +2\,\Gamma\,\sum_{si}\lambda_i\,(|V_{is}|^2\lambda_s - |V_{si}|^2\lambda_i). \tag{60}$$

The entropy expression can be recast as

$$\begin{aligned}\frac{dS}{dt} &= +\Gamma\,\sum_{si}|V_{si}|^2\lambda_i(\log_2\lambda_i - \log_2\lambda_s)\\ &\geq +\Gamma\,\sum_{si}|V_{si}|^2(\lambda_i - \lambda_s)\\ &\geq +\Gamma\,\sum_{si}\lambda_i(|V_{si}|^2 - |V_{is}|^2).\end{aligned} \tag{61}$$

We have used $x\log(x) \geq x-1$ to obtain the inequality above, with the result that

$$\frac{dS}{dt} \geq \Gamma\,\mathrm{Tr}\big[\,\rho(t)\,[L^\dagger(t), L(t)]\,\big].$$

Thus imposing the condition $[L(t), L^\dagger(t)] = 0$ yields $\frac{dS}{dt} \geq 0$, which is the known condition for obtaining increasing entropy from the Lindblad form.

Applying essentially the same steps to the purity

$$\begin{aligned}\frac{d\mathcal{P}(t)}{dt} &= -2\,\Gamma\,\sum_{si}|V_{si}|^2\lambda_i(\lambda_i - \lambda_s)\\ &\leq -2\,\Gamma\,\sum_{si}|V_{si}|^2(\lambda_i - \lambda_s)\\ &\leq -2\,\Gamma\,\sum_{si}\lambda_i(|V_{si}|^2 - |V_{is}|^2)\\ \frac{d\mathscr{P}(t)}{dt} &\leq -2\,\Gamma\,\mathrm{Tr}\big[\,\rho(t)\,[L^\dagger(t), L(t)]\,\big].\end{aligned} \tag{62}$$

For $[L(t), L^\dagger(t)] = 0$, we obtain decreasing purity $\frac{d\mathscr{P}(t)}{dt} \leq 0$ from the Lindblad form.

Above simple proofs show that for n_q qubits the Lindblad yields increased entropy and decreased purity with Lindblad operators that satisfy $[L(t), L^\dagger(t)] = 0$. The same procedure applies to Renyi, Tsallis, and other definitions of entropy.

Beretta [17] objects to the Lindblad form on the grounds that the entropy derivative diverges when the combination $\dot\lambda_i\,\log_2\lambda_j$ with $\dot\lambda_i \neq 0$ and $\lambda_j \to 0$ occurs. Based on this, even though it occurs for just a short time, he rejects the Lindblad form. Note this divergence is already contained in Eq. (24), as mentioned earlier. We nevertheless adopt a Lindblad form and simply avoid the occurrence of $\dot\lambda_i \neq 0$ and $\lambda_j \to 0$ by using the Lindblad to incorporate noise pulses that occur after the Beretta and Bath terms have already acted to increase the system's entropy, away from a pure one qubit state. That circumvents the problem for one qubit; the multi-qubit case remains an issue.

4.3.2. Steady Lindblad operator

To gain insight into the properties of the Lindblad form, we first consider steady, i.e. time-independent, Lindblad operators. Results for a master equation consisting of the unitary plus the Lindblad term only are shown in Figs. 8–12 for several simple steady Lindblad operators $L(t)$.

The first case is $L(t) = \sigma_x$, for which the polarization vector time dependence is given by: $\dot P_i = \sum_{j=1,3} M^{(1)}_{ij} P_j$, with

$$M^{(1)} = \begin{pmatrix} 0 & \omega_L & 0\\ -\omega_L & -2\,\Gamma & 0\\ 0 & 0 & -2\,\Gamma\end{pmatrix}. \tag{63}$$

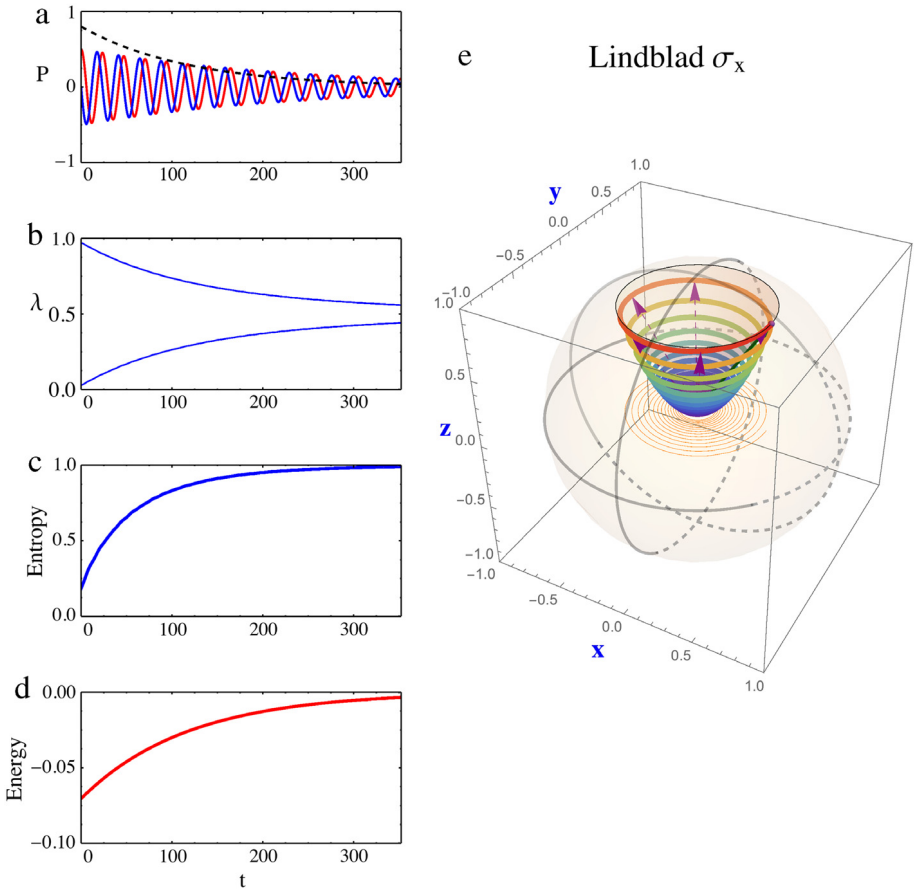

Fig. 8. Steady Lindblad. σ_x.

The polarization vector then varies as

$$
\begin{aligned}
P_x(t) &= e^{-\Gamma t}\left\{ P_x(0)\cos(\omega t) + \left(P_x(0)\frac{\Gamma}{\omega} + P_y(0)\frac{\omega_L}{\omega}\right)\sin(\omega t)\right\} \\
P_y(t) &= e^{-\Gamma t}\left\{P_y(0)\cos(\omega t) - \left(P_y(0)\frac{\Gamma}{\omega} + P_x(0)\frac{\omega_L}{\omega}\right)\sin(\omega t)\right\} \\
P_z(t) &= e^{-2\Gamma t}\, P_z(0),
\end{aligned}
\tag{64}
$$

with $\omega = \sqrt{\omega_L^2 - \Gamma^2}$.

The second case is $L(t) = \sigma_y$, for which the polarization vector time dependence is given by: $\dot{P}_i = \sum_{j=1,3} M^{(2)}_{ij} P_j$, with

$$
M^{(2)} = \begin{pmatrix} -2\,\Gamma & \omega_L & 0 \\ -\omega_L & 0 & 0 \\ 0 & 0 & -2\,\Gamma \end{pmatrix}. \tag{65}
$$

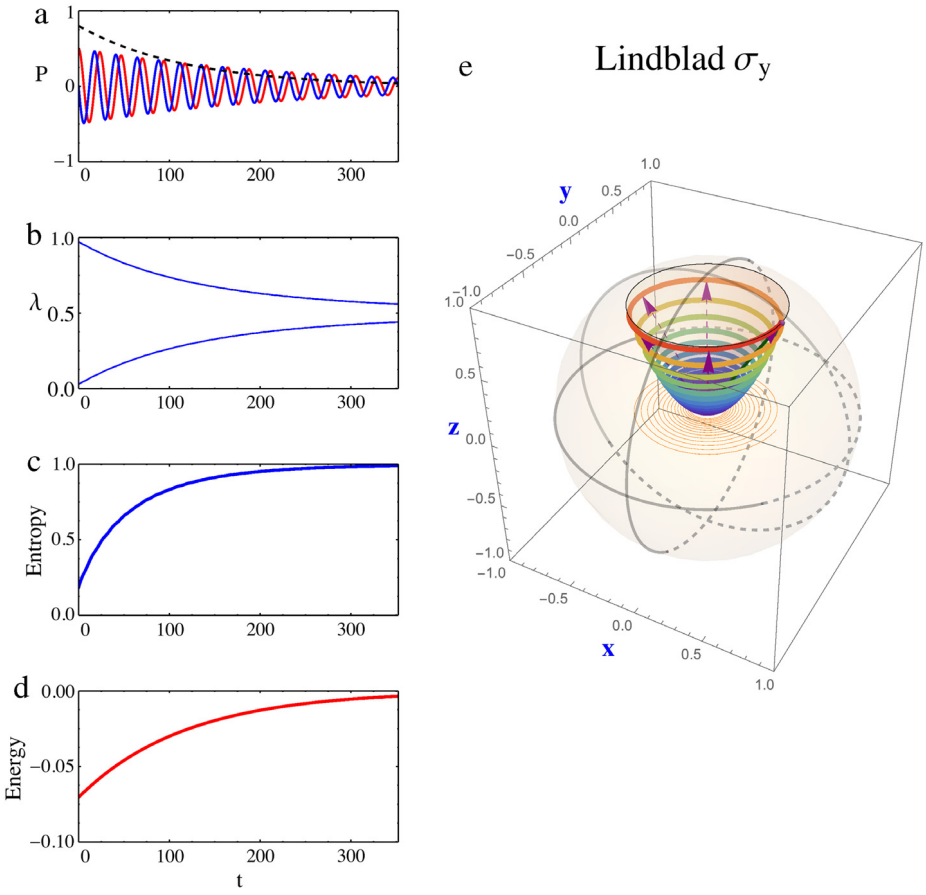

Fig. 9. Steady Lindblad. σ_y.

The polarization vector then varies as

$$P_x(t) = e^{-\Gamma t}\left\{P_x(0)\cos(\omega t) + \left(-P_x(0)\frac{\Gamma}{\omega} + P_y(0)\frac{\omega_L}{\omega}\right)\sin(\omega t)\right\} \tag{66}$$
$$P_y(t) = e^{-\Gamma t}\left\{P_y(0)\cos(\omega t) + \left(P_y(0)\frac{\Gamma}{\omega} - P_x(0)\frac{\omega_L}{\omega}\right)\sin(\omega t)\right\}$$
$$P_z(t) = e^{-2\Gamma t}\,P_z(0),$$

with $\omega = \sqrt{\omega_L^2 - \Gamma^2}$.

Next case is $L(t) = \sigma_z$, for which the polarization vector's time dependence is very simple: $\dot{P}_i = \sum_{j=1,3} M^{(3)}_{ij} P_j$, with

$$M^{(3)} = \begin{pmatrix} -2\,\Gamma & \omega_L & 0 \\ -\omega_L & -2\,\Gamma & 0 \\ 0 & 0 & 0 \end{pmatrix}. \tag{67}$$

The polarization vector then varies as

$$P_x(t) = e^{-2\Gamma t}\left\{P_x(0)\cos(\omega_L t) + P_y(0)\sin(\omega_L t)\right\} \tag{68}$$

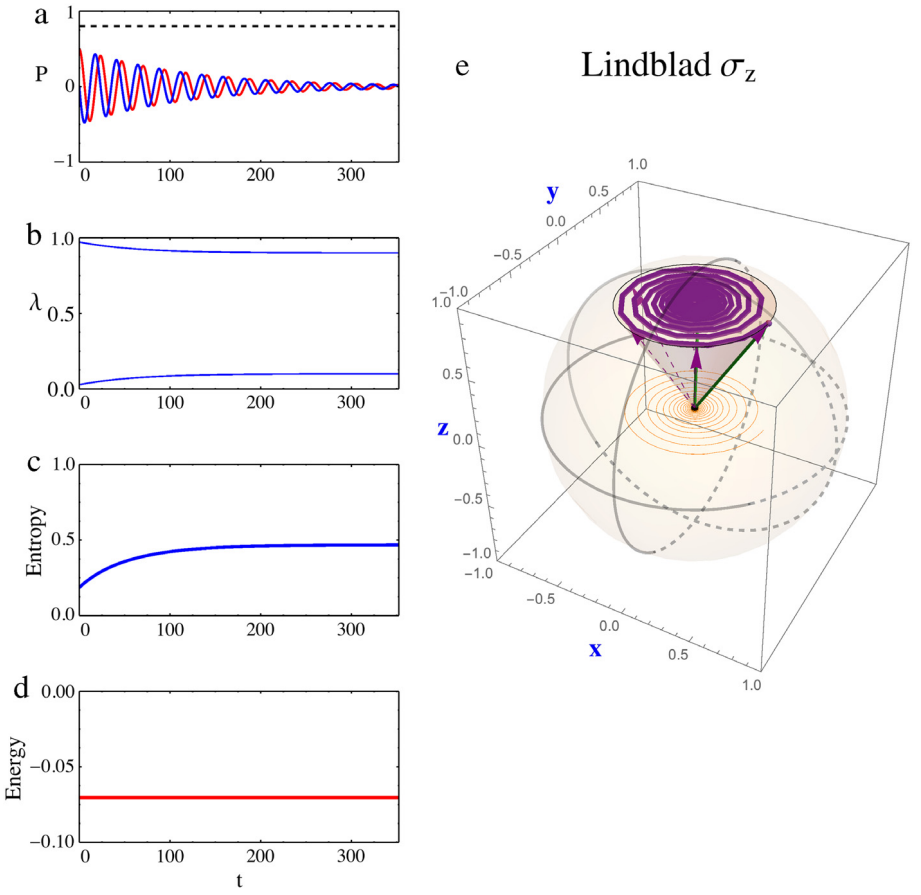

Fig. 10. Steady Lindblad. σ_z.

$$P_y(t) = e^{-2\Gamma t}\left\{P_y(0)\cos(\omega_L t) - P_x(0)\sin(\omega_L t)\right\}$$
$$P_z(t) = P_z(0).$$

All three of the above cases satisfy the condition $[L, L^\dagger] = 0$, and hence have increasing entropy and decreasing purity as displayed in Figs. 8–10.

Next case is $L(t) = \sigma_+ = \frac{\sigma_1 + i\sigma_2}{\sqrt{2}}$ for which the polarization vector's time dependence is $\dot{P}_i = \delta_{i3}\Gamma + \sum_{j=1,3} M^{(4)}_{ij} P_j$, with

$$M^{(4)} = \begin{pmatrix} -\frac{1}{2}\Gamma & \omega_L & 0 \\ -\omega_L & -\frac{1}{2}\Gamma & 0 \\ 0 & 0 & -\Gamma \end{pmatrix}. \tag{69}$$

The polarization vector then varies as

$$P_x(t) = e^{-\frac{1}{2}\Gamma t}\left\{P_x(0)\cos(\omega_L t) + P_y(0)\sin(\omega_L t)\right\} \tag{70}$$

$$P_y(t) = e^{-\frac{1}{2}\Gamma t}\Big\{P_y(0)\cos(\omega_L t) - P_x(0)\sin(\omega_L t)\Big\}$$
$$P_z(t) = 1 + e^{-\Gamma t}(-1 + P_z(0)).$$

Here we see that the z-component changes faster than the other components and increases with time from its initial value to one. The σ_+ is a lowering operator and drives the system towards a pure $|0\rangle$ state and thus decreases entropy. This decrease is also seen from $[L, L^\dagger] = +2\sigma_z$ and thus $\dot{S} \geq -2\Gamma P_z$.

Last case is $L(t) = \sigma_- = \frac{\sigma_1 - i\sigma_2}{\sqrt{2}}$ for which the polarization vector's time dependence is $\dot{P}_i = -\delta_{i3}\Gamma + \sum_{j=1,3} M^{(5)}_{ij} P_j$, with

$$M^{(5)} = \begin{pmatrix} -\frac{1}{2}\Gamma & \omega_L & 0 \\ -\omega_L & -\frac{1}{2}\Gamma & 0 \\ 0 & 0 & -\Gamma \end{pmatrix}. \tag{71}$$

The polarization vector then varies as

$$P_x(t) = e^{-\frac{1}{2}\Gamma t}\Big\{P_x(0)\cos(\omega_L t) + P_y(0)\sin(\omega_L t)\Big\} \tag{72}$$
$$P_y(t) = e^{-\frac{1}{2}\Gamma t}\Big\{P_y(0)\cos(\omega_L t) - P_x(0)\sin(\omega_L t)\Big\}$$
$$P_z(t) = -1 + e^{-\Gamma t}(1 + P_z(0)).$$

Here we see that the z-component changes faster than the other components and decreases with time from its initial value to minus one. The σ_- is a raising operator Fig. 1 and drives the system towards a pure $|1\rangle$ state. We now have $[L, L^\dagger] = -2\sigma_z$ and thus $\dot{S} \geq +2\Gamma P_z$, which is positive initially ($P_z > 0$) and turns negative after P_z flips to negative values.

These last two cases displayed in Figs. 11–12 do not satisfy the condition $[L, L^\dagger] = 0$, and their entropy and purity evolutions do not satisfy the $\frac{dS}{dt} \geq 0$ and $\frac{d\mathcal{P}(t)}{dt} \leq 0$ rules.

These various choices for Lindblad operators provide different behavior. For example, the $L = \sigma_z$ gives attenuation of the x and y polarization vectors and leaves the z component fixed. As we see later that case describes a system that has an increasing entropy at a fixed temperature. To model a system that evolves with fixed temperature, increasing entropy and no heat flow, we later turn to the Beretta form.

4.3.3. Lindblad projective measurement

The Lindblad operator represents a disturbance of the system due to outside effects. The act of measurement is an important outside effect in that a device is used to act on the system and to record its impact. As an example of how a Lindblad operator can represent the measurement process, we consider a one qubit system and its associated observable polarization vector. The Lindblad operator is assumed to be of the form

$$L = (\vec{\sigma}\cdot\vec{a})\,\theta_M(t) \tag{73}$$
$$\theta_M(t) = \frac{1}{2}\left\{\mathrm{Erf}\Big(\frac{t-t_1}{r}\Big) - \mathrm{Erf}\Big(\frac{t-t_2}{r}\Big)\right\},$$

where $\theta_M(t)$ is a pulse that equals one in the interval t_1 to t_2 with soft edges with a small $r = \tau_m/100$. This Lindblad pulse acts on the system during a short interval $\tau_m = t_2 - t_1$. The center of the pulse is at $t_0 \equiv \frac{t_1+t_2}{2}$, and the measurement is over at time $t_m = t_2$. The real unit vector $\vec{a} \equiv a_x\hat{n}_x + a_y\hat{n}_y + a_z\hat{n}_z \equiv \hat{m}$ is used to implement a measurement in the $\hat{m}$ direction. Note: $\int_{-\infty}^{\infty}\theta_M(t)\,dt = t_2 - t_1$.

In order to minimize any precession effect during the measurement, we need to have a very fast pulse with a strong Lindblad strength $\Gamma \gg \omega_L$.[9] We could simply stop the precession $\omega_L \to 0$, during the short measurement period τ_m. That stoppage could be implemented by a Hamiltonian bias pulse to generate temporary level degeneracy.

[9] The Beretta and Bath terms do not affect the measurement provided $\gamma_2 \ll \Gamma$ and $\gamma_3 \ll \Gamma$.

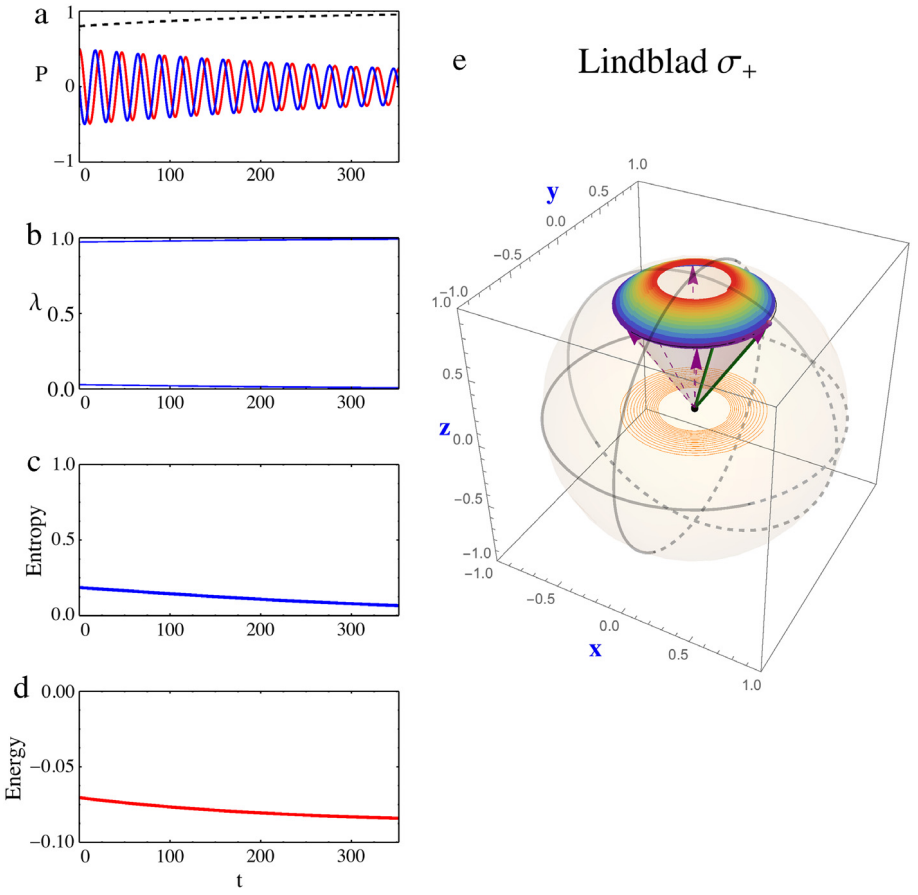

Fig. 11. Steady Lindblad: σ_+. This operator drives the system towards a pure $|0\rangle$ state.

Let us focus on how the polarization evolves during this measurement. The change in polarization vector is now (see the Appendix) for large Γ

$$\frac{d}{dt}\vec{P}(t) = -\vec{\omega}_L \times \vec{P}(t) + 2\,\Gamma\,\overrightarrow{\delta_P}(t) \to +2\,\Gamma\,\overrightarrow{\delta_P}(t) \tag{74}$$
$$\overrightarrow{\delta_P}(t) = \theta_M^2(t)(-\vec{P}(t) + (\vec{m}\cdot\vec{P}(t))\,\vec{m}).$$

We have set the Lindblad parameters as real $\alpha_i = a_i$ for $i = 1\ldots3$, and $\hat{a}.\hat{a} = 1$. The condition $[L^\dagger, L] = 0$ holds and thus the system's entropy increases during the measurement. A measurement along axis $\hat{m}$ becomes:

$$\frac{d}{dt}\vec{P}(t) = -2\,\Gamma\left\{\vec{P}(t) - (\hat{m}\cdot\vec{P}(t))\,\hat{m}\right\}\theta_M^2(t), \tag{75}$$

which displays the measurement property that the polarization in the measurement direction is unchanged in time, whereas the components in the other directions are reduced to zero rapidly. Inside the pulse time region the rule for one qubit is simply:

$$\frac{d}{dt}(\hat{m}\cdot\vec{P}(t)) = 0 \tag{76}$$

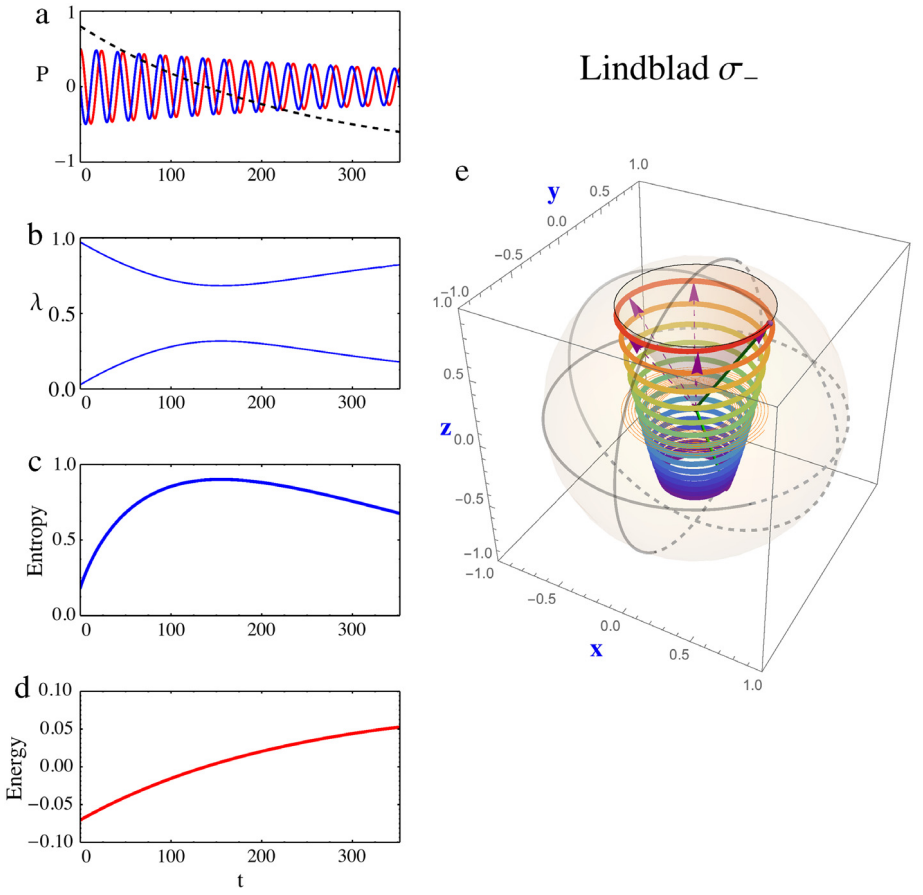

Fig. 12. Steady Lindblad: σ_- This operator drives the system towards a pure $|1\rangle$ state. Note here entropy first increases and then decreases.

$$\frac{d}{dt}(\hat{m}_\perp \cdot \vec{P}(t)) = -2\Gamma(\hat{m}_\perp \cdot \vec{P}(t)),$$

where $\hat{m}$ denotes the measurement direction and $\hat{m}_\perp$ directions perpendicular to the measurement direction. In the pulse time region, clearly $\hat{m} \cdot \vec{P}(t_m) = \hat{m} \cdot \vec{P}(t_1)$ & $\hat{m}_\perp \cdot \vec{P}(t) = e^{-2\Gamma(t-t_1)}\, \hat{m}_\perp \cdot \vec{P}(t_1)$, where t_1 is the measurement starting time. Here Γ is much larger than the Larmor frequency to assure rapid collapse of the density matrix under measurement. Thus the perpendicular component goes to zero rapidly at the end of the measurement t_m; to assure that limit the value of $\tau_m = t_2 - t_1$ is set equal to π/Γ. Then $e^{-2\Gamma(t_2-t_1)} = e^{-2\pi} \approx 0.0019$. To obtain a better zero a smaller τ_m can be used, but then the numerical evaluation requires increased precision.

The removal of perpendicular polarization components by measurement, shifts the one-qubit eigenvalues towards 1/2, with a corresponding increase in entropy and decrease in purity. The measurement is completed at time t_m when no further change occurs and the collapsed components have been removed. Therefore the final polarization is

$$\vec{P}_F = (\hat{m} \cdot \vec{P}_I)\, \hat{m}. \tag{77}$$

Measurement operator

The above Lindblad dynamical picture of measurement is equivalent to the Copenhagen version of density matrix collapse. The one-qubit operator for a projective measurement is in general

$$M_\alpha = |\alpha\rangle\langle\alpha| = \frac{1}{2}\Big\{(\sigma_0 + \vec{\sigma}\cdot\hat{m}_\alpha)\Big\}, \tag{78}$$

where $\hat{m}_\alpha$ denotes a measurement direction. For a projective measurement the states $|\alpha\rangle$ are orthonormal. Two sequential identical measurements $M_\alpha M_\alpha = M_\alpha$, are equivalent to one measurement. For two distinct measurements $\beta \neq \alpha$ $M_\beta M_\alpha = |\beta\rangle\langle\beta|\alpha\rangle\langle\alpha| = 0$. Thus for a basis of distinct measurements $M_\beta M_\alpha = \delta_{\beta\,\alpha} M_\alpha$. A complete set of measurements yields $\sum_\alpha M_\alpha = 1$. A simple example of these general remarks is taking $\alpha = \hat{m}$ and $\beta = -\hat{m}$. Compounding both of these measurements for polarization in the positive and negative $\hat{m}$ directions is used to construct a final state density matrix after such measurements.

In line with these remarks, the usual quantum rule for the final density matrix after projective measurement is

$$\begin{aligned}\rho_F &= \frac{\sum_\alpha M_\alpha \rho_I M_\alpha}{\mathrm{Tr}(M_\alpha \rho_I M_\alpha)} \\ &= \frac{\sum_\alpha (|\alpha\rangle\langle\alpha|)\,\langle\alpha|\rho_I|\alpha\rangle}{\sum_\alpha \langle\alpha|\rho_I|\alpha\rangle},\end{aligned} \tag{79}$$

where the state sum is over the $\pm\hat{m}$ directions. Note that the probability for a specific measurement is $\langle\alpha|\rho_I|\alpha\rangle = \mathrm{Tr}(M_\alpha\rho_I) = \frac{1}{2}(1 + \vec{P}_I\cdot\hat{m}_\alpha)$ and then the probability summed over both directions is $\sum_\alpha\langle\alpha|\rho_I|\alpha\rangle = 1$. Evaluation of the numerator, then gives the final density matrix

$$\begin{aligned}\rho_F &= |\hat{m}\rangle\langle\hat{m}|\frac{1}{2}(1 + \vec{P}_I\cdot\hat{m}) + |-\hat{m}\rangle\langle-\hat{m}|\frac{1}{2}(1 - \vec{P}_I\cdot\hat{m}) \\ &= \frac{1}{2}(\sigma_0 + \vec{P}_I\cdot\hat{m}(|\hat{m}\rangle\langle\hat{m}| - |-\hat{m}\rangle\langle-\hat{m}|)) \\ &= \frac{1}{2}(\sigma_0 + \vec{P}_I\cdot\hat{m}\,\vec{\sigma}\cdot\hat{m}) \\ \vec{P}_F &= (\hat{m}\cdot\vec{P}_I)\hat{m}.\end{aligned} \tag{80}$$

The final result shows that the usual measurement operator collapse is equivalent to a time-dependent Lindblad equation approach to measurement. If the Lindblad equation can be mapped to a stochastic Schrödinger equation, that would be an additional step towards a dynamic view of state collapse during measurement.[10]

A numerical example of a one-qubit Lindblad measurement is shown in Fig. 13. In this example the measurement is accomplished by a strong, fast Lindblad operator pulse ($\Gamma = 100\,\omega_L = 26.752$ GHz) in direction $\hat{m} = (\hat{x} + \hat{z})/\sqrt{2}$. The pulse starts at $t_1 = 2\,T_L = 46.973$ ns and ends at time $t_2 = t_1 + \tau_m = 47.091$ ns. The Larmor precession period ($T_L = 23.487$ ns) is much less than the pulse width ($\tau_m = \pi/(2\Gamma) = 0.117$ ns), which is set so negligible precession occurs during the measurement pulse. The initial polarization at $t = 0$ equals $(P_x(t_1), P_y(t_1), P_z(t_1)) = (0.2, 0.4, 0.8)$. The measurement is completed at time t_2 with a Lindblad operator $\theta_M(t)\,(\sigma_x + \sigma_z)/\sqrt{2}$. As expected, the polarization vector after this measurement collapses to $P_z = \vec{P}_x = .5$ and $P_y = 0$.

In Fig. 14, we take a closer look at the above measurement example. The left plot shows the initial precession, the rapid measurement starting at $t_1 = 2\,T_L == 46.97$ ns and the post-measurement precession. The measurement collapses the z and x components to equal values of 0.5; whereas, in the un-measured perpendicular $\hat{y}$ direction the polarization collapses to zero. Thereafter, normal

[10] S. Weinberg [23,24] has recently used the Lindblad equation to describe measurement from a more sophisticated view point which he suggests provides a conceptually improved starting point for formulating quantum mechanics. Also see [25,26] for earlier work based on a formulation of nonequilibrium quantum thermodynamics.

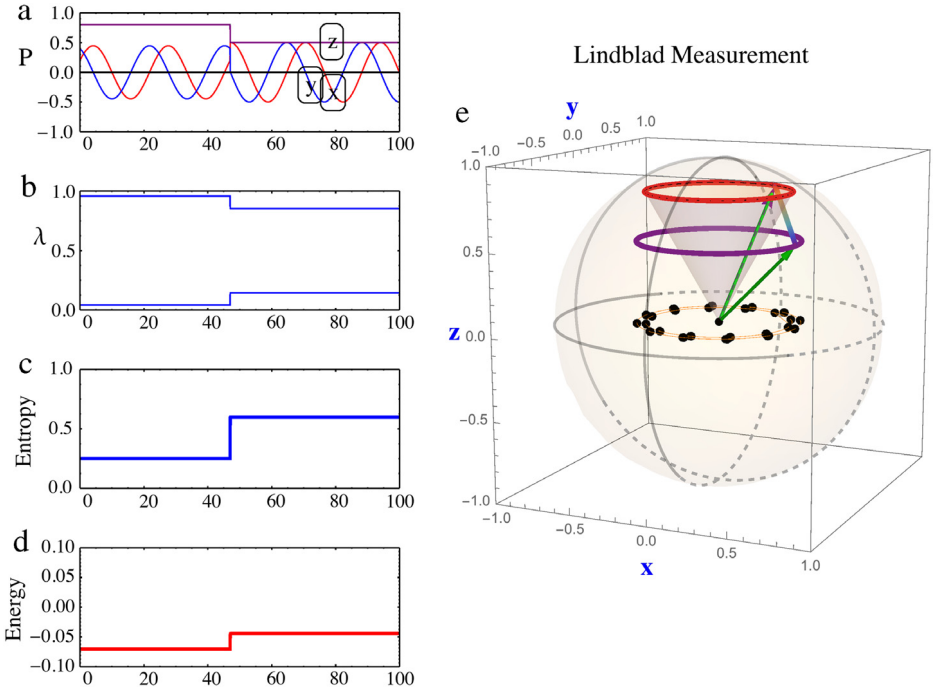

Fig. 13. Measurement as a strong Lindblad operator pulse. (a) Polarization vector evolution. Note after measurement polarization vector collapses to $\vec{P} = (\vec{P}_I \cdot \hat{m})\,\hat{m} = (0.50, 0.0, 0.50)$, with $P_y \to 0$. (b) Change in eigenvalues as expected from reduced magnitude of polarization vector; (c) Entropy increase due to measurement; (d) Energy change due to heat transfer; (e) Original precession cone followed by collapse to final (solid green) vector and continued precession. (For interpretation of the references to color in this figure legend, the reader is referred to the web version of this article.)

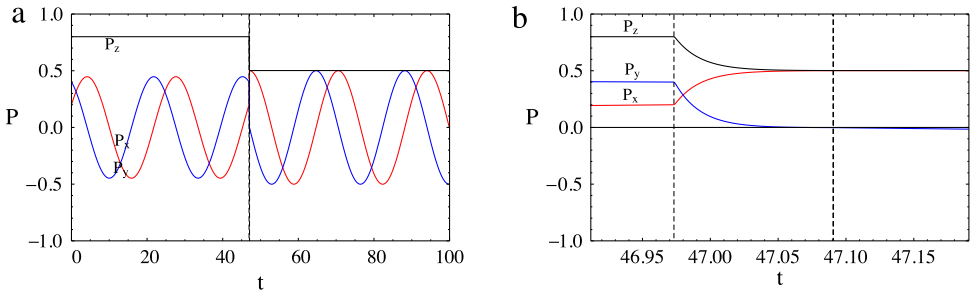

Fig. 14. The initial precession followed by the rapid measurement and then continued precession: (a) shows the evolution during the 0 to 100 ns time; (b) shows the detailed evolution during the t_1 to t_2 pulse (marked as vertical dotted lines). In both plots the initial polarization $(P_x(t_1), P_y(t_1), P_z(t_1)) \to (P_x(t_2), P_y(t_2), P_z(t_2))$ with $P_y(t_2) = 0$ and $P_x(t_2) = P_z(t_2) = (P_x(t_2) + P_z(t_2))/2$ as expected.

precession continues starting from the measured $P_x = P_z = .5, P_y = 0$ values after collapse. The right plot shows the details during the pulse with the vertical dotted lines indicating the start and end of the Lindblad pulse.

This procedure is readily generalized to multi-qubit, qutrit and hybrid cases, by extension to a wider range of polarization observables.

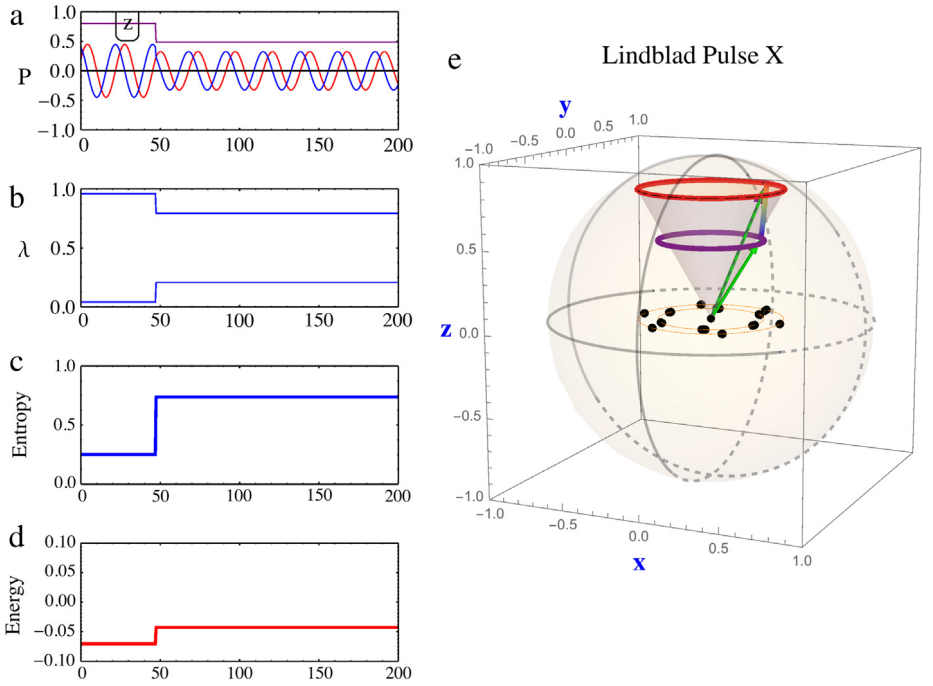

Fig. 15. Lindblad pulse $L(t) = \sigma_1\, \theta_L(t)$, acts from $t_1 = 46.97$ to $t_2 = 47.44$ ns. Strength $\Gamma = 2\,\omega_L = 0.535$ GHz was used to enhance the Lindblad pulse role. The initial polarization vector is {0.2, 0.4, 0.8}.

4.3.4. Noise Lindblad operator

We do not use steady Lindblad operators! Instead the Lindblad form is used only to incorporate noise pulses. If a noise pulse coincides in time with a gate pulse, we denote those cases as gate friction. It is possible to design time-dependent Lindblad operators that could drive the system to a specific equilibrium state or could describe a closed system that evolves with no heat transfer, but increasing entropy. These would be rather complicated Lindblad operators. It is much simpler to separate those effects into the Bath and Beretta terms, as we advocate. Thus in this treatment, the Lindblad form is only used to include random noise, gate friction and as described earlier, measurements.

Some simple examples of Lindblad pulses are now provided. The first Fig. 15 is a Lindblad pulse $L(t) = \sigma_1\, \theta_L(t)$, acting at a time t_0 with width τ_L. A simple soft square shape is used to introduce noise:

$$\theta_L(t) = \frac{1}{2}\left[\mathrm{Erf}\Big(\frac{t - t_1}{\tau}\Big) - \mathrm{Erf}\Big(\frac{t - t_2}{\tau}\Big)\right],$$

where $\int_{-\infty}^{\infty} \theta_M(t)\,dt = t_2 - t_1$, and $\theta_M(t_0) = 1$, along with Γ set the strength of the pulse. Fig. 16 provides a closer look at the action of this Lindblad operator during its pulse. During the pulse, the z and y polarizations are reduced and the x component is unchanged, which is reflected in the increase of entropy and the eigenvalue motion towards equality seen in Fig. 15.

The second example Fig. 17 consists of four σ_1 noise pulses of fixed strength $L(t) = \sigma_1 \sum_{i,1,4} \theta_L(t - \Delta_i)$, acting at a times $t_0 + \Delta_i$ with fixed width τ_L.

Finally, we present a case Fig. 18 with eight random Lindblad pulses each of general form $\vec{\alpha} \cdot \vec{\sigma}$. In that complex case periods of entropy decrease as well as increase occur. In general, the Lindblad pulse set is designed to simulate the extant noise impacting the system.

In the above cases there are no gates, just Lindblad noise.

These are preliminary tests of the stability of quantum memory under the intrusion of noise. The stability of quantum memory is illustrated in Fig. 19 where the dependence of Fidelity on the Lindblad

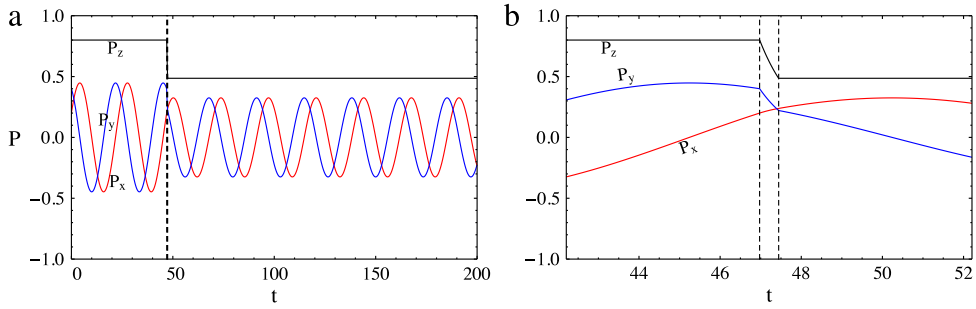

Fig. 16. View of Lindblad pulse $L(t) = \sigma_1\, \theta_L(t)$ (a) over the 0 to 200 ns time span (b) during the pulse period. Vertical dashed lines indicate pulse start $t_1 = 46.97$ ns and finish at $t_2 = 47.44$ ns. Change of polarization due to this Lindblad pulse is given by $\delta\vec{P} = -2\,\Gamma\,\{0, P_y, P_z\}$, see the Appendix. Again $\Gamma = 2\,\omega_L$ enhances the Lindblad pulse role. The initial polarization vector is {0.2, 0.4, 0.8}.

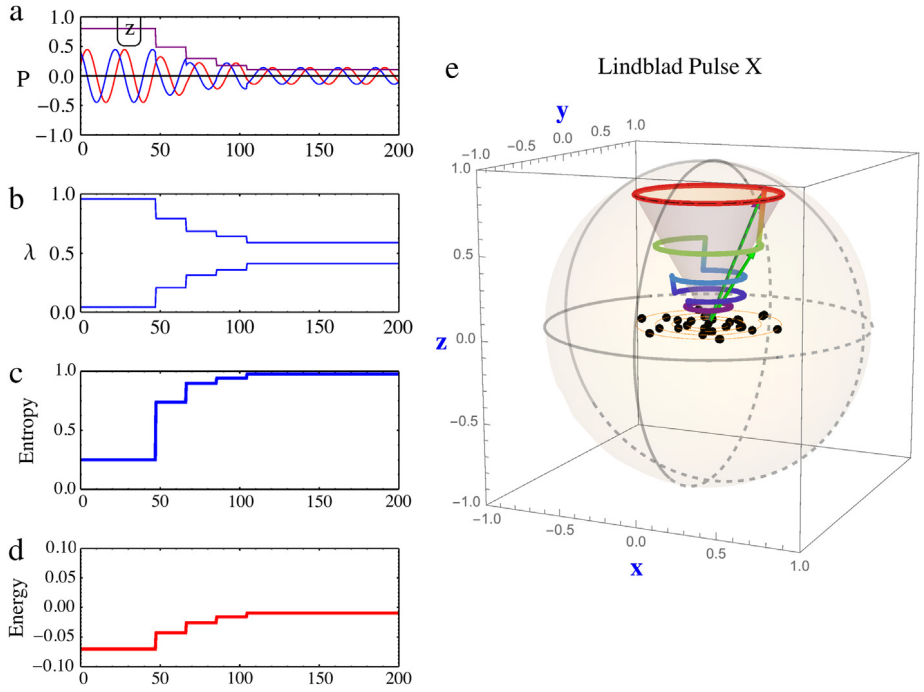

Fig. 17. Four equi-spaced Lindblad pulses $L(t) = \sigma_1\, \theta_L(t)$, acting from $t_1 = 46.97$ ns to $t_f = 104.7$ ns, of width 0.47 ns. A large $\Gamma = 2\,\omega_L$ was used to enhance the Lindblad pulse role. The initial polarization vector is {0.2, 0.4, 0.8}.

strength is displayed. The two density matrices used in the fidelity are $\rho(t)$ at $t_1 = 2T_L$ and at a final Larmor grid time after the noise abates, t_f = Mod[tend, T_L] $\times$ T_L, i.e. on the Larmor time grid. This procedure can set limits on allowed noise to maintain a stable density matrix. Later memory stability will also be tested including the Beretta and Bath terms.

In all cases, we use a positive strength $\Gamma \geq 0$ for the Lindblad noise model. However, it has been noted in the literature [30] that a negative $\Gamma \leq 0$ can simulate non-Markov effects. This would represent an environment that is affected by the system and after a delay feeds back some of the

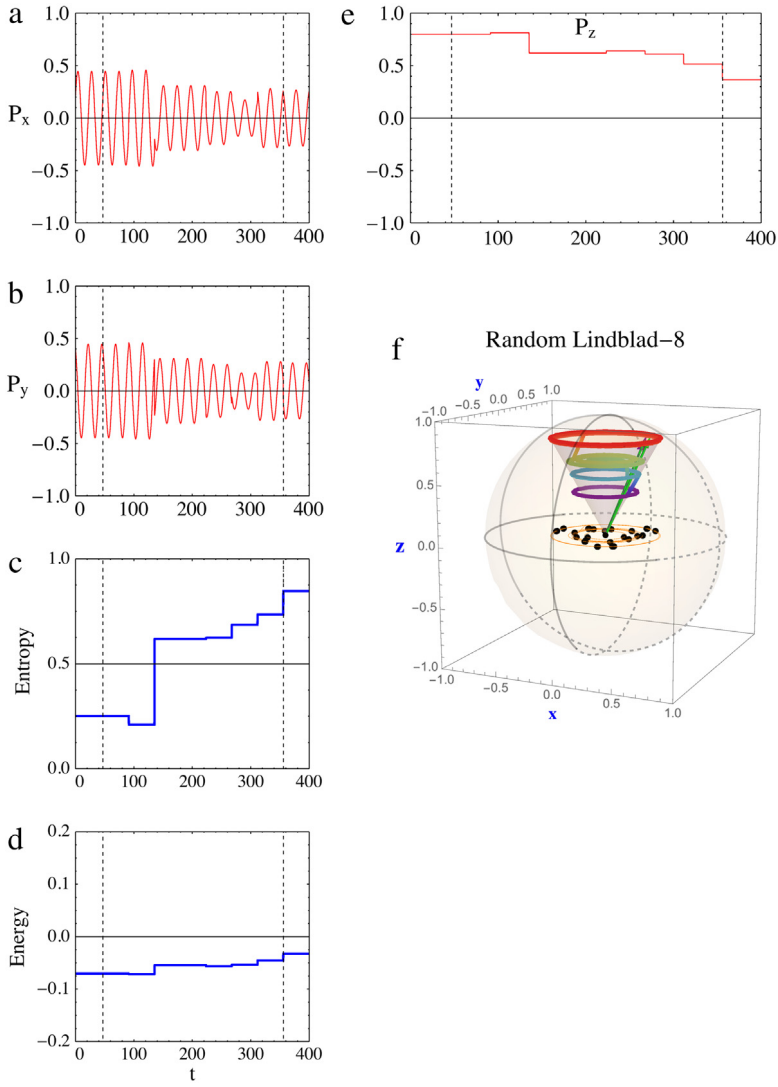

Fig. 18. Eight random Lindblad pulses of width 0.47 ns acting at equally spaced time intervals during $t_1 = 46.97$ ns to $t_f = 355.9$ ns. Each pulse is of form $L(t) = \vec{\alpha} \cdot \vec{\sigma}\theta_L(t)$, with complex random $\vec{\alpha}$. Note that the entropy decreases in intervals when $[L^\dagger, L] \neq 0$. Vertical dotted lines indicate the start of the first and end of the last pulse. A large $\Gamma = 2\,\omega_L$ was used here to enhance the Lindblad pulse role. The initial polarization vector is {0.2, 0.4, 0.8}.

information to the system, thereby ameliorating the detrimental effects of noise. This kind of feedback is well known in the optical model of nuclear reactions as formulated by projection operator methods. Design of such an environment could be the key to achieving stable memory and operations in a QC. This will be explored in a future study.

4.3.5. Gates plus Lindblad operators

In addition to evolution of a non-degenerate system subjected to Lindblad noise, we can include quantum gates. The cases of a NOT gate and then of a Hadamard gate along with three subsequent random noise pulses are shown in Fig. 19. As a figure of merit, the fidelity, evaluated on the Larmor

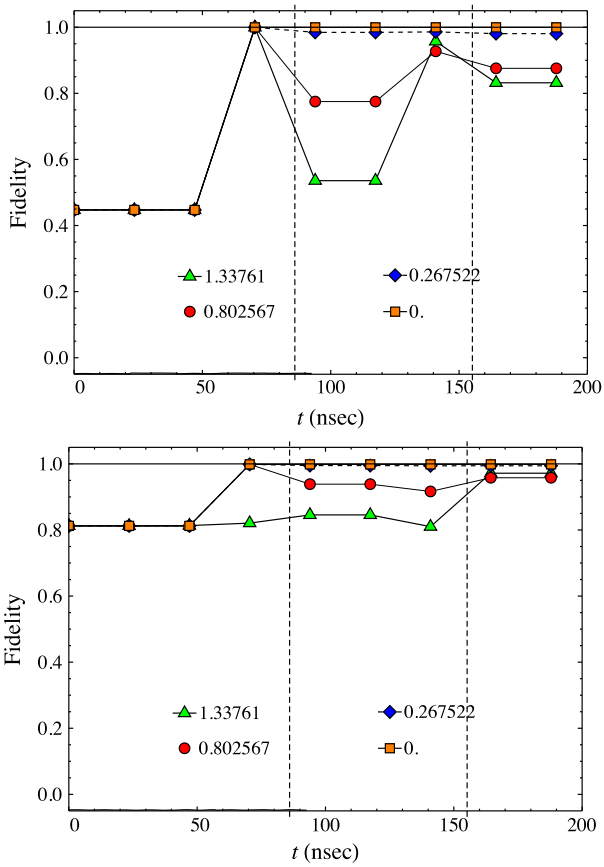

Fig. 19. Top(Not), Bottom(Hadamard) gates followed by three random Lindblad pulses at equally spaced time intervals. Gate pulse is from $t_1 = 46.97$ ns to $t_2 = 47.443$ ns, of width 0.47 ns. Lindblad pulses are $L(t) = \vec{\alpha} \cdot \vec{\sigma}\theta_L(t)$, with complex random $\vec{\alpha}$. Vertical dotted lines mark start/end of the Lindblad noise. Different $\Gamma's$ show effect of noise on the gate fidelity. Symbols are on the Larmor period grid.

period T_L grid is displayed in Fig. 19 for various Lindblad strengths Γ, which illustrates how noise can affect efficacy and how to ascertain the allowed noise level to accomplish a simple process.

4.4. Equilibrium-closed system

Now let us consider the case of unitary evolution, absent noise but subject to the Beretta term $\mathscr{L}_2$. For a simple initial state as stipulated in Table 1, we see in Fig. 20 that for a closed system as described by $\mathscr{L}_2$, the entropy increases uniformly and no heat is transferred. This is accomplished by a steady reduction of the polarization vector components in directions perpendicular to the axis associated with the level splitting, in this case the $\hat{z}$ axis. Since both P_x & P_y decrease, while P_z remains fixed, it follows that the entropy increases and the purity decreases since they both depend on the length of the polarization vector, which gets reduced. The temperature of the system is dictated by the unchanging P_z component, so the closed system has a fixed temperature determined by the initial condition. That is consistent with the no heat transfer property of the Beretta term.

Fig. 21 shows the same situation when a Not gate is included.

These statements generalize to multi-qubit and qutrit system, which involve more spin observables.

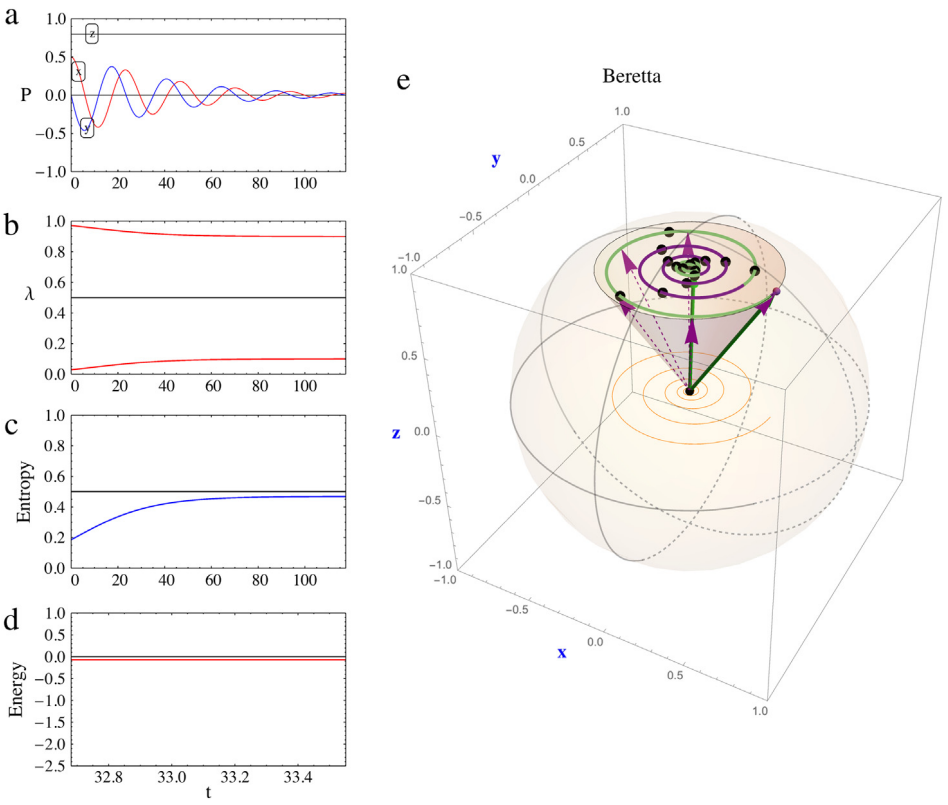

Fig. 20. Density matrix evolution with unitary plus Beretta closed-system term. The polarization in the z-direction stays fixed, while the perpendicular components decay. No energy flows into or out of the system and the temperature is fixed by the initial value. The entropy increases steadily.

4.5. Equilibrium-thermal bath

In Fig. 22, the case of unitary evolution absent gates, but with a Korsch (K) type bath $\mathscr{L}_3$ is shown. The temperature of the bath is stipulated by setting $T = 0.273$ K and thus $\beta = \frac{1}{k_B T} = 0.0425\,(\mu\text{eV})^{-1}$. Since T is higher than the temperature obtained from the initial density matrix $T_0 = 0.00093$ K, heat flows into the system, polarization moves closer to zero, entropy goes closer to 1. (When the bath temperature is lower than the initial temperature T_0, heat flows out and the final z-polarization is larger than the initial value.) The final equilibrium density matrix is of Gibbs form, as expected.

In Fig. 23, a special comparison of Korsch(K) and Beretta(B) cases are compared for the same situation, T_Q was selected[11] to give similar results for the polarization, entropy, and energy evolutions. Recall that for a (B) bath the ratio $\dot{Q}/\dot{S}$ is held fixed by T_Q, while the parameter $\boldsymbol{\beta_3(t)}$ is state and hence time-dependent; while, for a (K) bath $\boldsymbol{\beta_3(t)}$ is kept fixed, but the $\dot{Q}/\dot{S}$ ratio varies with time as seen in Fig. 23. The $\dot{Q}'$, $\dot{S}$ and $\dot{Q}/\dot{S}$ display interesting differences. A rescaling $\dot{Q}' = 8.2\dot{Q}$ is used for a closer look at the detailed evolution, where for (B) the energy and entropy rates are instantaneously correlated. This seems a correct property for an ideal bath, in contrast to a time lag between an entropy rate peak followed by a later energy transfer peak as seen for the Korsch case. The (K) shows a smooth and substantially increasing $\dot{Q}/\dot{S}$, but an expected steady value for the (B) bath. The net change in

[11] The value of T_Q was set by the overall ratio $(Q(t_f) - Q(0))/(S(t_f) - S(0))$, where the final values are determined by β_3.

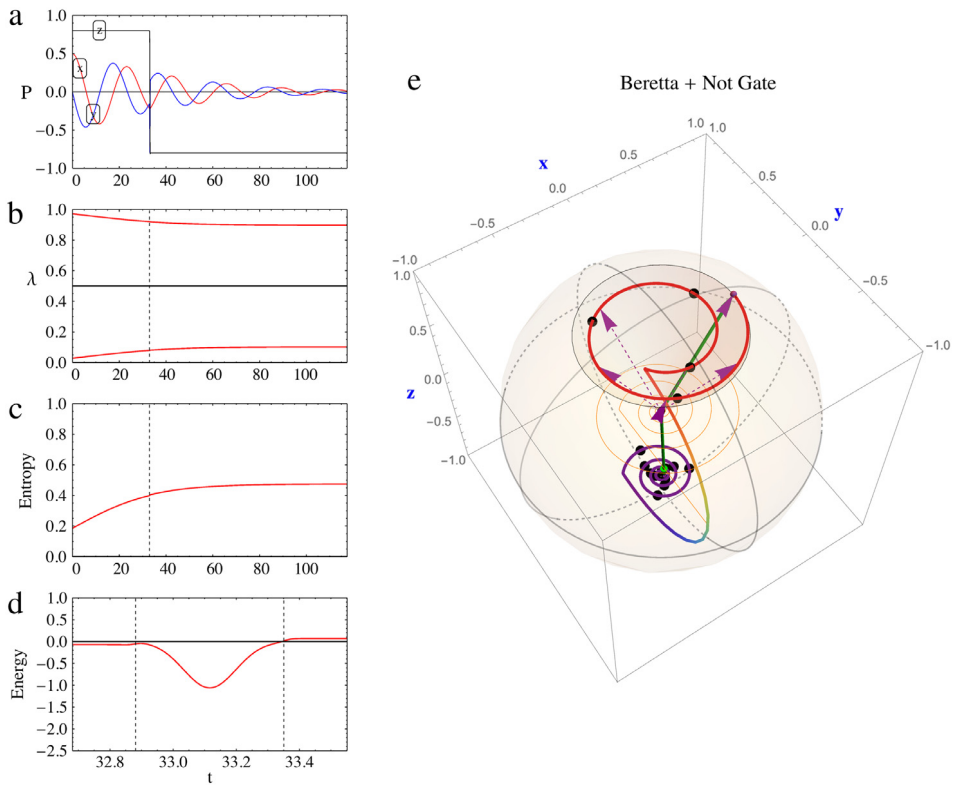

Fig. 21. Density matrix evolution with unitary evolution including a Not gate, plus the Beretta closed-system term. The polarization in the z-direction flips, while the perpendicular components decay. Energy of the system changes because of the Not gate. The entropy increases steadily. Temperature experiences an inversion. Vertical dashed lines indicate the start and end times of the Not gate.

energy and in energy are the same for both cases by design. Note that equilibrium is reached somewhat earlier for the (B) bath.

4.6. Equilibrium—thermal bath plus Lindblad

To gain additional insight concerning the Beretta (B) bath density matrix evolution, consider a simple case with no gates, and steady Lindblad operators of either σ_- or σ_+ form; these are compared in Fig. 24. The $\dot{Q}/\dot{S}$ ratio now consists of the fraction[12]

$$\frac{\dot{Q}}{\dot{S}} = \frac{\dot{Q}_1 + \dot{Q}_2 + \dot{Q}_3}{\dot{S}_1 + \dot{S}_2 + \dot{S}_3} = \frac{\dot{Q}_1 + \dot{Q}_3}{\dot{S}_1 + \dot{S}_2 + \dot{S}_3} \to \frac{\dot{Q}_1 + \dot{Q}_3}{\dot{S}_1 + \dot{S}_3}, \tag{81}$$

where the closed system term is now omitted (when on, it has: $\dot{Q}_2 = 0$, and $\dot{S}_2 > 0$).

For a σ_- Lindblad term Fig. 12, $\dot{Q}_1$ is positive and decreasing and $\dot{S}_1$ starts positive, decrease to zero at $t \approx 40$ ns, then goes to a small negative value. For a σ_+ Lindblad term Fig. 11, both $\dot{Q}_3$ and $\dot{S}_3$ are both negative decreasing. Meanwhile, the (B) bath contributions have positive $\dot{Q}_3, \dot{S}_3$.

For σ_+, starts positive and becomes negative as the upper level gets more occupied and the entropy heads for zero. Recall that a σ_- Lindblad first increases the entropy and then drives it towards zero,

[12] The subscript labels are 1: Lindblad, 2: closed system, 3: Bath.

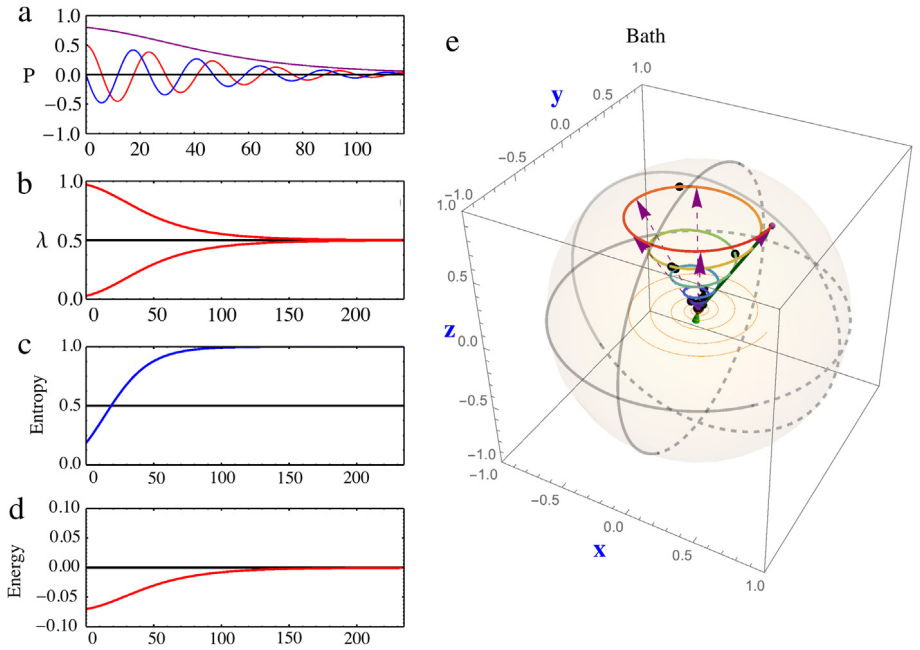

Fig. 22. Evolution with unitary plus Korsch bath terms. Bath temperature is $T = 0.273$ Kelvin and initial state temperature is $T_0 = 0.00093$ Kelvin. Equilibrium eigenvalues are both close to 1/2, corresponding to a maximum entropy of almost 1. The final polarization vector is $\bar{P} = \{0, 0, 0.0037\}$, which is determined by the bath $T = 0.273$ Kelvin.

while also flipping the z-polarization. In contrast the σ_+ Lindblad depopulates the upper level and drives the entropy down from its original value, with a corresponding increase in the z-polarization.

As a result of these properties, the denominator changes sign when the Lindblad entropy slope becomes strong enough to exceed the positive bath entropy rate of increase.

As a result, the $\frac{\dot{Q}}{\dot{S}}$ changes sign and deviates from its steady value where such cancellations occur. The up–down–up spike for σ_-, near 62 ns and the down–up–down spike for σ_+, near 70 ns follow from the differing $\dot{Q}_1$, $\dot{Q}_3$ and $\dot{S}_1$, $\dot{S}_3$ signs and trajectories near the entropy nodal regions. It would be interesting to see if such flips appear with realistic noise.

5. One qubit system and the full model master equation

The full model master equation includes unitary evolution with gate pulses, the Lindblad $\mathscr{L}_1$ with noise pulses, the Beretta $\mathscr{L}_2$ to describe a closed system, and a bath $\mathscr{L}_3$ term to include contact with a bath of fixed temperature. This provides a flexible model that can be used to gain insight into QC dynamics and gauge the requisite condition for a successful QC process. We give a simple example here, with additional cases and tools to be posted.

5.1. Full master equation not gate

In Fig. 25, a full model master equation case is displayed with a single Not gate. The initial polarization $\bar{P} = \{0.2, 0.4, 0.8\}$ precesses about the z-axis with a Larmor angular frequency of $\omega_L = 0.2675$ GHz. Eight random equi-spaced Lindblad pulses act during the $t = 46.9$ to 531 ns interlude; the overall Lindblad strength is set as $\Gamma = 0.4\,\omega_L$. At 46.9 ns a Not gate acts. The Beretta (closed system) strength is set as $\gamma_2 = .01\,\omega_L$, The bath term strength $\gamma_3 = .005\,\omega_L$, and the bath temperature is 27.3 K. The evolution of the polarization shows a P_z gate flip followed by attenuation

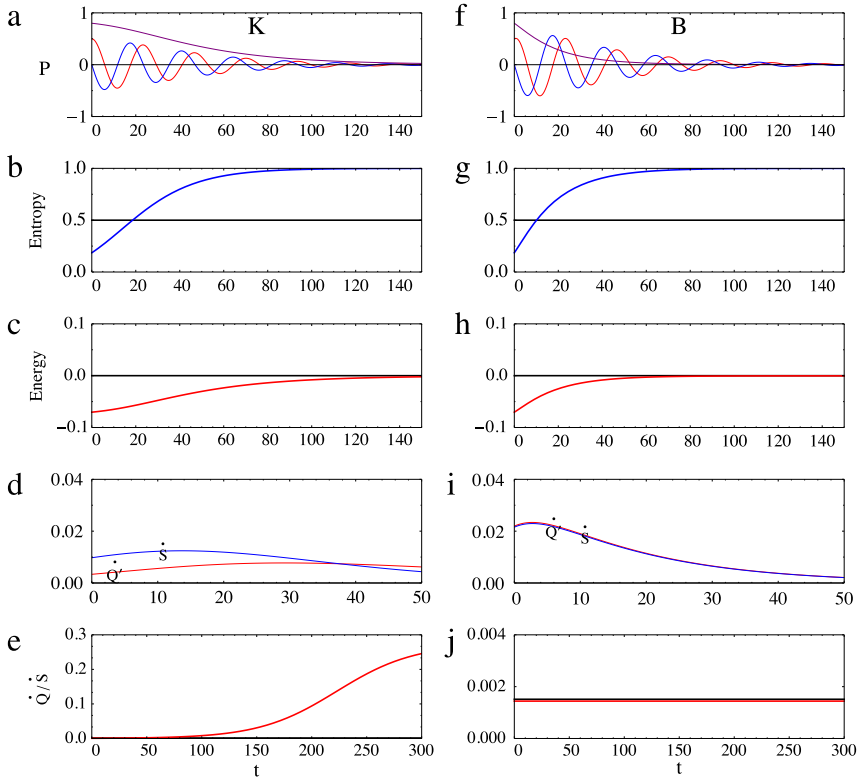

Fig. 23. Comparison of the Korsch (K) and Beretta (B) baths. Here there are no gate, Lindblad or closed system terms. The Beretta clearly displays a steady value for $\dot{Q}/\dot{S}$ of $k_B T =$. The Korsch bath has a constant value $\beta_3 =$, but the $\dot{Q}/\dot{S}$ is very different. Energy unit is μeV and time in nsec. Note: Beretta bath equilibrates first.

and noise alterations, as expected. The Lindblad noise shows up as jagged entropy evolution, where the random nature of the Lindblad pulses allows for entropy decreases as well as increases. The energy plot shows the Not and bias pulse work and the energy flip to increased energy occupation.

In Fig. 26, the fidelity, entropy and purity evolutions are presented with values on the Larmor grid (integer multiples of T_L) indicated by red dots (fidelity), blue diamonds (entropy) and orange squares (1-purity). There is a clear reduction in fidelity due to noise and gradual fall off from the Beretta and bath effects. Both entropy and purity reveal the affect of Lindblad noise.

In Fig. 27, the case of two sequential Not gates is shown. Studies of other gate sequences and alternate noise scenarios reveal similar properties. Cases of no gates, but noise, Beretta and bath terms can be used to identify quantum memory losses.

6. Conclusions and future steps

6.1. Conclusions

The main result from this study is the design of a dynamical density matrix model that incorporates the essential features of a quantum computer. Although much of the input is well-known, it is shown here how to implement unitary gate pulses, plus an associated bias pulse, to replicate the usual quantum gates. The bias pulse is introduced to obviate the accumulation of detrimental phase accumulations due to qubit non-degeneracy. To replicate the QC static gate network for a sequence

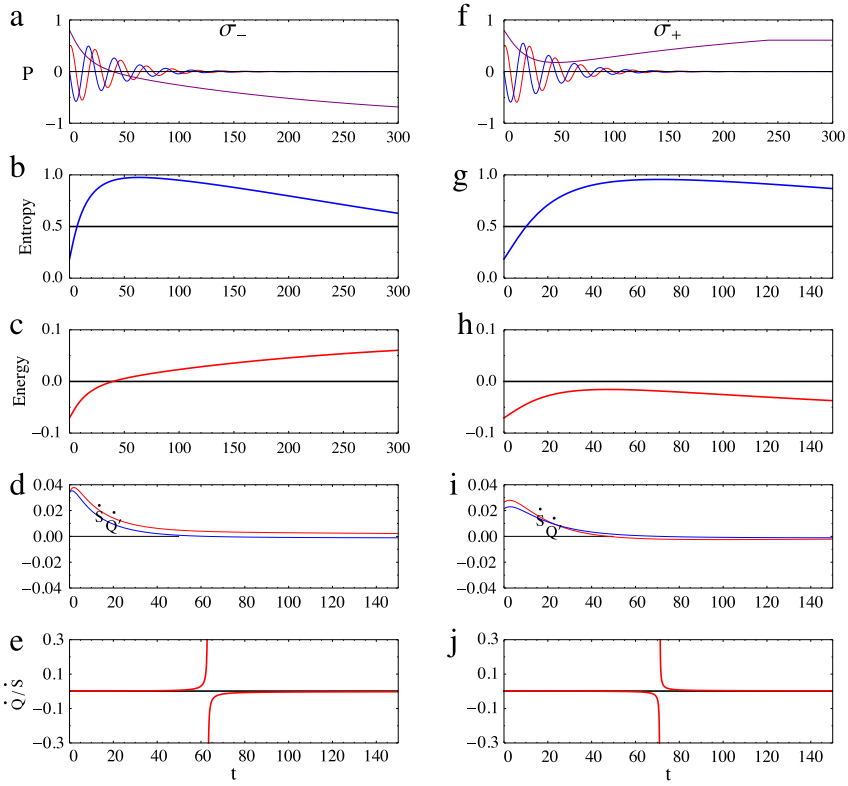

Fig. 24. Sample result for a Beretta (B) bath with steady σ_- and σ_+ Lindblad operators. Here gate and closed system terms are omitted. The Beretta displays a steady value for $\dot{Q}/\dot{S}$ except in $\bar{\dot{S}}_1 + \bar{\dot{S}}_3 \to 0$ regions induced by $\sigma_\pm$ Lindblad operators.

of gates, it is shown that the various gates also need to be applied on the Larmor time grid. The model also includes dissipative, decoherence and thermodynamic effects. The Lindblad addition to unitary dynamics has the essential feature of maintaining the unit trace, Hermiticity and positive definite nature of the evolving density matrix. A general Lindblad form, after examining various static Lindblad operators, is used to incorporate random noise and gate friction effects; these are input as non-static pulses. In addition, strong rapid Lindblad operators are implemented as measurements, and the associated restriction to be valid measurements examined. Although many other effects can also be cast into Lindblad form, it is much simpler to design separate forms for closed systems and for system–Bath interactions. The closed system form is one developed by Beretta based on a general study of non-equilibrium thermodynamics. Two types of system–Bath interactions are examined, one that has been studied before, and another one also originated by Beretta that is illustrated herein to have physical advantages. Another result of this study is provided by several examples of how to apply the full model including random noise, gate friction, closed system entropy increase, and system–Bath interactions to a set of unitary gates. Fidelity is used to gauge the stability of such a QC setup. This illustrates how the model can be used as a tool to examine and design valid experiments to achieve stable quantum computation.

6.2. Future steps

Clearly, there is much more to explore. Extension to two or more qubit systems is planned along the lines delineated in this work, as well as generalization to qutrit and hybrid qubit/qutrit systems.

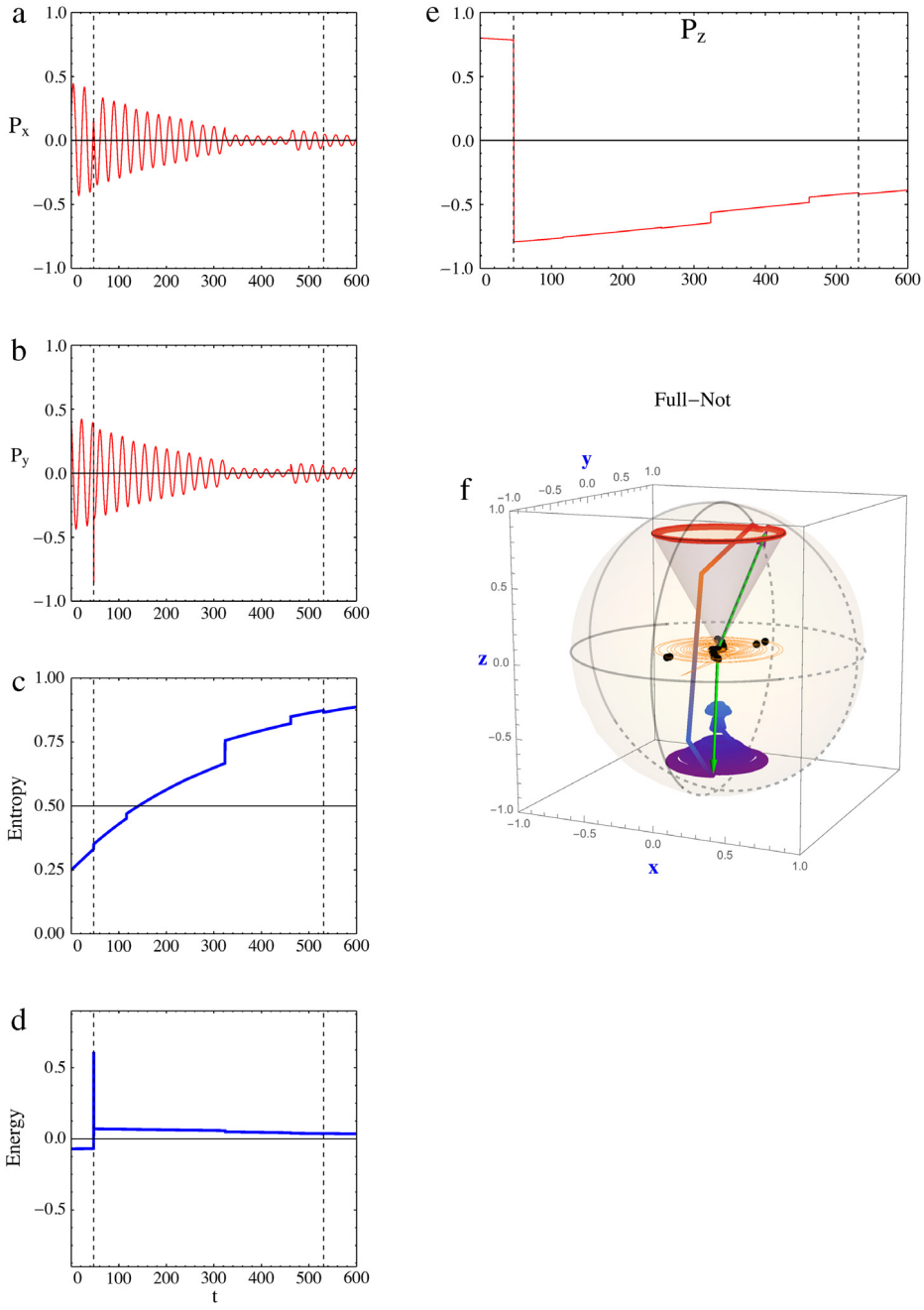

Fig. 25. A Full master equation case with a Not gate, Lindblad noise and Beretta and Bath terms.

Application to small Carnot and Otto cycle qubit engines would aid in clarification of non-equilibrium dynamics and of non-ideal QC [31,32]. Such studies will be greatly influenced by the preferred choice of a Beretta type bath model.

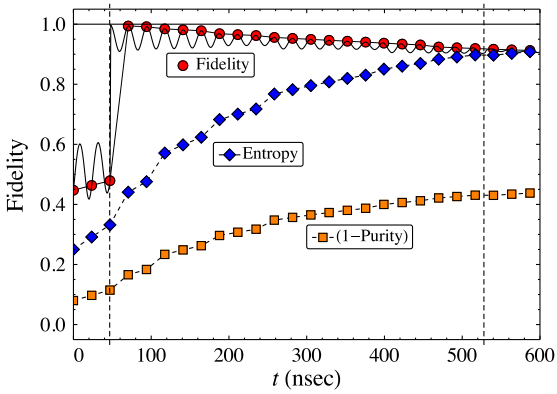

Fig. 26. Fidelity with a Not gate, noise and Beretta and Bath terms. Between the vertical dashed lines eight Lindblad noise pulses occur. Fidelity, entropy and purity are shown on the Larmor period grid. The full master equation density matrix is compared to the expected $\rho_e = \sigma_1 \cdot \rho(0) \cdot \sigma_1$, by examining the Fidelity($\rho(t)$, ρ_e). The fidelity jumps to one after the gate, then drifts down due to noise, Beretta and Bath terms.

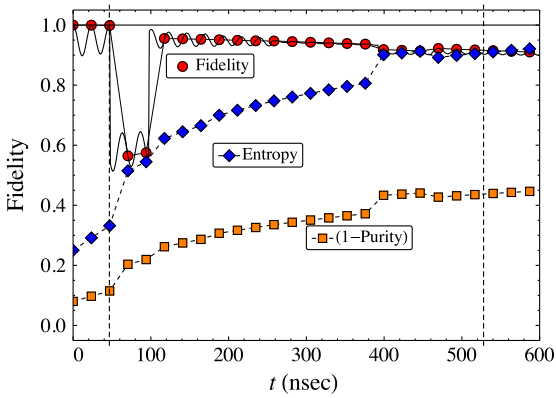

Fig. 27. Fidelity for two sequential not gates, Beretta and bath terms as in Fig. 26. Noise occurs between the vertical dashed lines, but differs from prior plot. After the second not gate, the fidelity does not equal 1, due to the noise, Beretta and bath effects.

Lindblad pulses as measurement operators warrant further exploration. One possibility is to generate a stochastic Schrödinger equation that approximates this density matrix model, as a means of exploring quantum wave function collapse. Of course, the main application should be to QC algorithms using realistic parameter settings based on extant experiments to explore the requisite conditions for good fidelity results. Error correction methods can also be evaluated for their efficacy.

It might also be possible to invent pulses or chirps to simulate non-Markovian dynamics as a potential mechanism for enhancing QC memory and algorithm efficiency.

It is hoped that the methods explored here will help in these directions.

Acknowledgments

We gratefully acknowledge the participation of Dr. Yangjun Ma and Dr. Victor Volkov at an early stage of this work. One of the reviewers enhanced this paper considerably by excellent suggestions and in-depth insights, for which the author is deeply grateful. The figures for this article have been created using the SciDraw-LevelScheme scientific figure preparation system [M.A. Caprio, Comput. Phys. Commun. 171, 107 (2005) and http://scidraw.nd.edu]. The author also thanks Prof. Edward

Gerjuoy for stressing the need to examine non-degenerate qubits, and Dr. Robert A. Eisenstein for encouragement and excellent advice during the completion of this paper.

Appendix. One-Qubit Lindblad in simplified form

To gain insight into the effect of the Lindblad operators on the evolution of the density matrix as stipulated by the motion of the polarization vector, let us generate the equation for the time dependence of $\vec{P}(t)$. The general form of the Lindblad term is

$$\mathscr{L}_1 = \Gamma\ \overrightarrow{\delta_P}(t) \cdot \vec{\sigma} \tag{A.1}$$

where $\overrightarrow{\delta_P}(t)$ is a real vector in (x, y, z) spin space. That form arises from the fact that $\mathscr{L}_1$ is a traceless and Hermitian scalar. Our task is to express $\overrightarrow{\delta_P}(t)$ in terms of the Lindblad parameters α_i.

The first step in extracting that result is to take the ensemble average

$$\begin{aligned} \frac{d}{dt}\mathrm{Tr}\Big[\vec{\sigma}\,\rho(t)\Big] &= \mathrm{Tr}\Big[\vec{\sigma}\,\frac{d}{dt}\rho(t)\Big] = \frac{d}{dt}\vec{P}(t) \\ \frac{d}{dt}\vec{P}(t) &= -\frac{i}{\hbar}\mathrm{Tr}\Big[\vec{\sigma}\Big[H(t),\,\rho(t)\Big]\Big] + \mathrm{Tr}\Big[\vec{\sigma}\,\mathscr{L}_1\Big]. \end{aligned} \tag{A.2}$$

For a Hamiltonian $H \equiv -\frac{\hbar}{2}\,\omega_L\,\vec{\sigma}\cdot\hat{h}$, the first term in Eq. (A.2) becomes

$$-\frac{i}{\hbar}\mathrm{Tr}\Big[\vec{\sigma}\,\Big[H(t),\,\rho(t)\Big]\Big] = -\omega_L\,\hat{h}\times\vec{P}(t),$$

which yields a Larmor precession of the polarization vector about the direction $\hat{h}$. We then have

$$\frac{d}{dt}\vec{P}(t) = -\omega_L\,\hat{h}\times\vec{P}(t) + 2\,\Gamma\,\overrightarrow{\delta_P}(t). \tag{A.3}$$

For the second term in Eq. (A.2) , after inserting the expansions of both the density matrix and the Lindblad and taking the traces, one arrives at the following result:

$$\begin{aligned} \overrightarrow{\delta_P}(t) = &-a^2\,[\vec{P}(t) - (\hat{a}\cdot\vec{P}(t))\,\hat{a}] - b^2\,[\vec{P}(t) - (\hat{b}\cdot\vec{P}(t))\,\hat{b}] \\ &+\vec{P}(t)\times(a_0\,\vec{b} - b_0\,\vec{a}) + 2(\vec{a}\times\vec{b}). \end{aligned}$$

We have expressed the eight complex Lindblad parameters $\alpha_0, \vec{\alpha}$ in terms of eight real quantities by the definition $\alpha_j = a_j + i\,b_j$ for $j = 0\ldots 3$. Recall that $L = \alpha_0\,\sigma_0 + \vec{\alpha}\cdot\vec{\sigma}$.

The three components of the vector $\overrightarrow{\delta_P}(t)$ give the change in the associated component of the polarization vector induced by the Lindblad term and allows one to identify how the Lindblad coefficients (and the corresponding Pauli operators) affect the motion of the polarization vector within the Bloch sphere. For example for $b_0 \to 0$, and $\vec{b} \to 0$ the result simplifies to

$$\overrightarrow{\delta_P}(t) \to -a^2\,[\vec{P}(t) - (\hat{a}\cdot\vec{P}(t))\,\hat{a}], \tag{A.5}$$

which yields a reduction in the polarization components in the direction perpendicular to $\hat{a}$. For $\hat{a}$ in the x–y plane, this would take a polarization vector precessing about say the z-axis[13] and move it into the Bloch sphere in a spiral motion towards a limit of zero polarization or maximum entropy. This is clearly a dissipative or friction situation.

Eq. (A.3) also gives the time derivative of $\vec{P}(t)\cdot\vec{P}(t)$, as

$$\begin{aligned} \frac{d}{dt}\vec{P}(t)\cdot\vec{P}(t) &= 2\,\vec{P}(t)\cdot\frac{d}{dt}\vec{P}(t) \\ &= 4\,\Gamma\,\vec{P}(t)\cdot\overrightarrow{\delta_P}(t) \\ &= 4\,\Gamma\,\{-a^2\,\mathbf{P}^2[1-(\hat{a}\cdot\hat{n})^2] - b^2\,\mathbf{P}^2[1-(\hat{b}\cdot\hat{n})^2] + 2\,a\,b\,(\hat{a}\times\hat{b})\cdot\vec{P}\,\}. \end{aligned} \tag{A.6}$$

[13] In this case, we have assumed that the Hamiltonian is of the simple form $H = -\frac{\hbar}{2}\,\omega_L\,\vec{\sigma}_3$.

Since $(\hat{a}\cdot\hat{n})^2$ and $(\hat{b}\cdot\hat{n})^2$ are both less than 1, the first two terms reduce **P**. The third term contributes only when $(\hat{a}\times\hat{b})\neq 0$, and it can be positive or negative. Since $[L, L^\dagger] = 4\,a\,b\,(\hat{a}\times\hat{b})\cdot\vec{\sigma}$, we see that the polarization vector decreases when $[L, L^\dagger] = 0$, but can increase when $[L, L^\dagger]\neq 0$. since the purity, entropy and eigenvalues depend only on **P**, this shows that purity decreases, entropy increases and eigenvalues move towards 1/2, when $[L, L^\dagger] = 0$, and purity can increase, entropy can decrease and eigenvalues can move towards 1 and 0, when $[L, L^\dagger]\neq 0$. For example, when $\vec{a} = n_x/\sqrt{2}$, and $\vec{b} = \pm\, n_y/\sqrt{2}$, the third term becomes $\pm 2\,a\,b\,P_z$, which increases **P** when $\pm P_z > 0$ and decreases **P** when $\pm P_z < 0$. This explains the numerical results for the role of Lindblad operators.

The role of each Lindblad operator, as stipulated by the a_j, b_j parameters, can thus be understood based on Eq. (A.3). Eq. (A.5) plays an important role when Lindblad is a measurement operator.

The eight real parameters $a_j, b_j, j = 0\ldots 3$ are used as time-dependent pulses to simulate external dissipative and decoherence effects.

References

[1] M.A. Nielsen, I.I. Chuang, Quantum Computation and Quantum Information, Cambridge University Press, 2000.
[2] J. Preskill, Preskill's Quantum Computation lectures, Physics 219 Course Information. URL http://www.theory.caltech.edu/%7Epreskill/ph219/index.html#lecture.
[3] E. Joos, H.D. Zeh, C. Kiefer, D. Giulini, J. Kupsch, I.-O. Stamatescu, Decoherence and the Appearance of a Classical World in Quantum Theory, second ed., Springer, Berlin, 2003.
[4] J.A. Wheeler, W.H. Zurek, Quantum Theory and Measurement, Princeton University Press, 1983.
[5] K. Hornberger, Entanglement and Decoherence: Foundations and Modern Trends, Springer, Berlin, Heidelberg, 2009, pp. 221–276.
[6] K. Kraus, States, Effects and Operations: Fundamental Notions of Quantum Theory, Springer, Verlag, 1983.
[7] H. Carmichael, Statistical Methods in Quantum Optics 1: Master Equations and Fokker-Planck Equations, Springer, Berlin, 1999.
[8] R. Alicki, D.A. Lidar, P. Zanardi, Phys. Rev. A 73 (2006) 052311.
[9] S.L. Adler, Phys. Lett. A 265 (2000) 58–61.
[10] A. Peres, Phys. Rev. A 61 (2000) 022116.
[11] A. Kossakowski, Rep. Math. Phys. 3 (1972) 247.
[12] G. Lindblad, Comm. Math. Phys. 48 (1976) 2.
[13] V. Gorini, A. Kossakowski, E.C.G. Sudarshan, J. Math. Phys. 17 (1976) 5.
[14] G. Lindblad, Non-Equilibrium Entropy and Irreversibility, second ed., Reidel, Dordrecht, Berlin, 1983.
[15] G.P. Beretta, Rep. Math. Phys. 64 (2009) 139–168.
[16] G.P. Beretta, Int. J. Quantum Inf. 5 (2007) 249–255.
[17] G.P. Beretta, J. Phys. Conf. Ser. 237 (2005) 1–32.
[18] H.J. Korsch, H. Steffen, J. Phys. A 20 (1987) 3787.
[19] M. Hensel, H.J. Korsh, J. Phys. A 25 (1992) 2043.
[20] J. Neumann, R.T. Beyer, Mathematical Foundations of Quantum Mechanics, Princeton university press, 1955.
[21] L. Landau, Z. Phys. 45 (1927) 5.
[22] U. Fano, Rev. Mod. Phys. 29 (1957) 74.
[23] S. Weinberg, Phys. Rev. A 90 (2014) 042102.
[24] S. Weinberg, Rev. A 93 (2016) 032124.
[25] G.N. Hatsopoulos, E.P. Gyftopoulos, Found. Phys. 6 (15–31) (1976) 561–570.
[26] J.L. Park, Amer. J. Phys. 36 (1968) 211, also: R.F. Simmons Jr., J.L. Park, Found. Phys. 11 (1981) p. 47 and p. 297.
[27] B. Juliá-Díaz, J.M. Burdis, F. Tabakin, Comput. Phys. 174 (2006) (2016) 914–934, also see: Comput. Phys. Comm. 180 (2009) 474; Comput. Phys. Comm. 182 (2011) 1693; and Comput. Phys. Comm. 201, 171.
[28] N.F. Ramsey, Phys. Rev. 103 (1956) 20.
[29] S. Braun, J.P. Ronzheimer, M. Schreiber, S.S. Hodgman, T. Rom, I. Bloch, U. Schneider, Science 339 (2013) 6115.
[30] S. Bhattacharya, A. Misra, C. Mukhopadhyay, A.K. Pati, Phys. Rev. A 95 (2017) 012122.
[31] R. Alicki, J. Phys. A: Math. Gen. 12 (5) (1979) L103.
[32] D. Gelbwaser-Klimovsky, W. Niedenzu, G. Kurizki, in: Advances in Atomic, Molecular, and Optical Physics, vol. 64, Academic Press, 2015, pp. 329–407.